Ecole Nationale Supérieure Louis Lumière
Master Photographie - Promotion 2023

Study of film texture : Grain, Halation and Rendition of Details.

Researching image processing pipelines restoring materiality to digital images.

Master's thesis

Clément Montmea

Supervision

Pascal MARTIN, applied optics professor, ENS Louis-Lumière.

Sean COOPER, Senior Color Scientist, ARRI

Jury members

Véronique FIGINI, lecturer in history of photography.

Pascal MARTIN, university professor at ENS Louis-Lumière.

Sean COOPER, Senior Color Scientist, ARRI

Alain SARLAT, professor of sensitometry and colorimetry, ENS Louis-Lumière

Olivier PATRON, Digital Imaging Technician (DIT), Freelance

Carried Out at: Arnold & Richter Cine Technik GmbH (ARRI)

Submission date: December 7th, 2023

Acknowledgements

This thesis was conducted at Arnold and Richter Cine Technik in Munich and has been supervised by Sean Cooper, Senior Color Scientist at ARRI. I would like to thank Sean Cooper for the supervision of the work as well as Harald Brendel, Tamara Seybold, and Jeffrey W. Hagerman for having me on their teams. Thanks to Dimitri Kloster from the optic team for his help on MTF measurements, Laurent Gudman and Benjamin Herb for their feedback and help during data acquisition. More broadly, I would like to thank the image science team as well as the optic, testing and support department at ARRI that helped me with the data acquisition and measurement.
I would like to thank my supervisor, Pascal Martin, for his advice and direction of this thesis, Stéphanie Solinas and Anne-Lou Buzot for their input for the practical work of the thesis. I thank ENS Louis-Lumière for the support and the opportunity to attend CIC31.
Finally, I would like to address a special thanks to Alain Sarlat without whom, none of this would have been possible.

For the documentary photo series displayed in practical work, I would like to thank Arlette Maussan, Jacques Renoud et Jean-Claude Bareille who took me around to visit the local mining exploitation. Thanks to Benjamin Bergnes for his advice when preparing for the upcoming tour.
Finally, I would like to thank my family and more specifically my parents for their support. A special thank goes to Jean Gibert and Elisa Bapst for their constant help and support since this project began.

Abstract

Study of film texture: Grain, Halation and Rendition of Details explores an aesthetic and technical question relevant to the worlds of photography and cinema. The lack of colorful and spatial attributes linked to digital sensors pushes photographers and cinematographers to return to a film capture medium. This latent image in the crystal structure is developed in chemical baths, revealing the image captured by the camera. These millions of silver particles, of different sizes, as well as the support and structure of film will make this image a material object by essence. These coincidences and technical imperfections brought by the materiality of the medium are key to the textures and colors of film images. This work seeks to delineate to what extent those characteristics can be mimicked in digital images. Via physical measurements, the original processes will be analyzed to be better described and understood. Then, image processes will be crafted and tested to achieve various types of textures from grain to halation. Color, without being the main focused question of the work, will come alongside this thesis as it influences the displayed image. Finally, results will be analyzed and controlled via visual inspection and reviewed alongside objective measurements.

Based on the particular attention given to materiality in this thesis, the practical part, *Omnipresence de la Mine,* will document mining and its consequences. We will explore French and German landscapes in search of Mines' traces of the past, present, and future.

Contents

4 - Measuring film texture

Introduction

In cinematography and photography, the term *texture* historically refers to attributes of the captured scene: grass, piece of fabric, object composed of small patterns... However, texture could account for characteristics that do not depend on the scene captured by the camera but on the capturing device itself. As a matter of fact, due to their materiality and physical base, films possess texture features such as grain and halation. When exposed to light, they embed their physical characteristics in the resulting image. Furthermore, linked to the materiality of this photographic process, randomness must be embraced as it is directly created from the inherent structure of film halides in the emulsion. Digital cameras, on the other hand, are less unpredictable as they are organized in a mosaic array with fixed borders and numbers of sensitive elements in this case photosites. This thesis defines film texture in terms of grain, rendition of detail and halation and presents a processing pipeline[1] to restore these features brought by the physicality of film to digital cameras.

As always at ENS Louis-Lumière, the preparation of the thesis started during the second year when looking for a relevant subject of study for the diploma. As a photographer, I was interested in exploring the film look (color-wise) as well as film scanning. For those coming from a cinema background, it has to be stated that in photography there are no up-to-date devices to scan color negative films properly aside from the Fujifilm Frontier and Noritsu Scanners. To be clearer, there are many scanners available on the market, but none of them satisfies the needs in terms of scanning photographic film. For example, the spectral sensitivities of the devices used are either too broad, or the scanning speed is not high enough or the sharpness does not even show film grain properly.
Looking into this matter, cinema film scanners are better suited to capture the material they were designed for. The ARRISCAN is equipped with narrowband

[1]A processing pipeline is a set of data processing elements connected in series

LEDs for the illuminant paired with a monochromatic sensor with a high resolution, is equipped with a sharp macro lens and scans film at a speed of around a frame per second. Furthermore, while acquiring data more thoughtfully, the ARRISCAN handles the rest of the color processing pipeline with data-crafted transforms which I was highly interested in. At that time, I had basic knowledge of color science and image processing and was eager to learn more about it.
Alain Sarlat knew Harald Brendel (Chief of Image Science at ARRI) from a former research he had conducted on the ARRI Alexa system and put me in contact with him. We understood that the scanner department was not an option for my upcoming thesis but that he would be glad if I wanted to work on image textures and more specifically on film textures.
After a conference call, we agreed on my master's thesis topic and the time frame it should be accomplished. A seven and a half month internship was scheduled during my last year second semester at ARRI in Munich in the Image Science department. The internship would require image processing and color science knowledge to be properly conducted.

It has to be stated in this introduction that the École Nationale Supérieure Louis-Lumière doesn't have a class specifically tackling image processing. Louis-Lumière is a school more focused on image technics rather than image science. The class coming close to this discipline is the Sensitometry and Colorimetry class, where we learn the basis of image science from capture to screen, both in digital and analog. Other classes (especially in the cinema department) are more focused on the cinema industry needs in terms of image technicians such as Directors of Photography, Gaffers, Colorists and DITs.
To be more prepared for my internship at ARRI, I took classes for a semester at Sorbonne Université - Pierre et Marie Curie as the university has a 2-year master's program on Image processing under the responsibility of Isabelle Bloch.

The master thesis work started after a month and a half of getting familiar with the ARRI processing pipeline and tools. I had to get familiar with ARRI's in house developed tools implemented in Matlab for research and development. I worked on a previously acquired film dataset to craft color transforms as well as extract grain

characteristics. I got familiar with color corrections based on 3x3 matrices, as well as root polynomial matrices and 3D LUT creation. Furthermore, I explored Noise Power Spectra analysis as well as halation geometric simulation. We finally started to think about how we should acquire our dataset, both for spatial and color characteristics as well as assessment data. Data acquisition protocols needed to be validated through tests we did on black and white film (at least for the spatial data and more specifically the rendition of detail in question).
At the end of this internship period, we started elaborating processing protocols to restore materiality to the ARRI Alexa35 digital images. These algorithms had to be based on scientific measurements of film texture features and should reproduce visually the so-called "film look" in spatial terms.

Throughout this internship as well as during the master's thesis work, we settled upon defining film texture around three key characteristics that are Grain, Rendition of Detail and Halation. Each of the characteristics is subdivided into a set of parameters that will be introduced in the Background section and studied throughout the thesis, more specifically in the Analysis section.
ARRI being one of the leading brands in high-end cinema, we wanted to explore this Texture topic with solid knowledge in different fields of image science to make educated guesses and decisions. The topic involved both spatial and color processing and a good understanding of film sensitometry, colorimetry and developing chain. Furthermore, photographic skills such as operating a film camera and developing black and white film were very useful skills to carry out the thesis properly. Learning and creating new tools was rewarding and challenging and allowed us to study the Texture question in depth and more thoroughly.
This thesis work is a comprehensive presentation of what has been done and achieved in terms of data acquisition, data analysis and image processing for the past six months.

1. Background

This section is meant to set common foundations with the reader that will be relevant for the understanding of this thesis. These foundations will be mainly technical, both from the physical acquisition and the image processing part. This background will lay the basis of both digital and film.
The first section will tackle the physical acquisition of light for different capturing mediums. This part will exhibit the main differences in texture signature in the different acquisition techniques.
The second section will tackle the signal processing from the raw image to the screened image. This section will focus on how a standard image processing shapes the viewed images in terms of texture, color and gradation. Spatial processing will also be discussed in this section as well as metrics that will be used later.
The third section will give an overview of what is known and researched in terms of our three identified texture components.
The last two sections will introduce the processing pipelines and the principles used by our two main acquisition devices, the ARRI Alexa35 and the ARRISCANXT.

1.1 Image acquisition

1.1.1 Digital Image Acquisition

Digital cameras register an image thanks to their sensor, composed of individual photosites. The light hitting the sensor is then converted to an electric charge proportional to the number of photons captured. The electrical current is then digitized thanks to an analog-to-digital converter (ADC). There are two main families of digital sensors which are CCD and CMOS[2]. The latter is nowadays the

[2] RWG Hunt, *The Reproduction of Colour*, p.555

most used out of the two, thanks to its increased dynamic range and low power consumption. The total sum of charges accumulated throughout the exposure time is then converted to a voltage, which is amplified and then digitized.

The camera described in the paragraph above is only monochromatic and only sensitive to the changing intensity of light. Its spectral sensitivity covers more than the visible spectrum without differentiating short mid and long wavelengths. UV and IR filters are used in front of the photosites to block out non-visible wavelengths captured by the sensor. In a single sensor camera, a CFA (type Bayer)[3] filters the light with an alternating pattern composed of 3 bandpass filters, red green and blue. This trichromatic principle mimics the human visual being itself based on it. The CFA single sensor image recovers its full color information by spatial interpolation at the demosaicing stage (see section 1.2). Each photosites and dyes concatenated with its optical stack (UV/IR filters and micro-lenses) has a given spectral sensitivity that will define its response to light and more importantly its color rendition[4] . The Color Processing pipeline presented in the upcoming section is made to modify the raw spectral sensitivity and match it to the human vision also defined as the CIE 1931 Standard Observer.

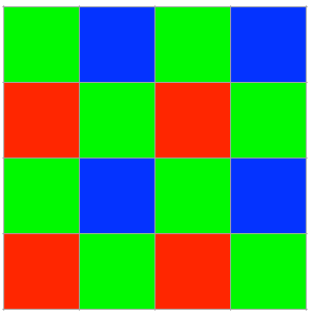

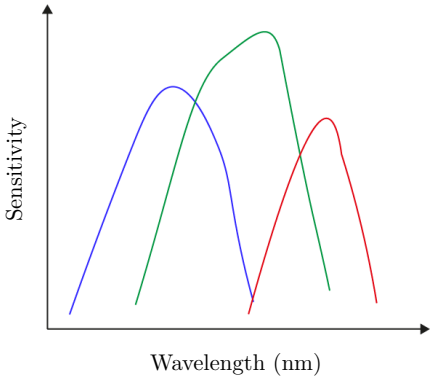

Figure 1 - Bayer Matrix & Sensor spectral sensitivity

1.1.2 Analog Film

Analog films are a technology relying on silver or metallic halide sensitive to light. The sensitive crystals are put in suspension in an organic base that is primarily

[3] Edward J. Giorgianni, *Digital color management : encoding solutions, p.20-21*

[4] *ibid.*.

composed of gelatinous compounds in the films used by the motion picture industry. Even if they are part of the analog process family, other metallic photographic mediums like cyanotype, tintype and other compounds like albumin or Arabic gum will not be reviewed.

Black and White Film

Black and White films are composed of a gelatinous compound loaded with a mixture of Silver Halides (usually a blend of Silver Bromide and Chloride). Several factors affect each crystal's sensitivity to light such as its type (chloride/bromide), its size and its shape. Additional parameters such as depth into the emulsion layer will affect the grain sensitivity[5] (relative to the amount of light measured at the film surface). Lastly, the developing chemicals as well as conditions and techniques used to develop the film.

Each silver crystal exposed to light will yield a binary outcome after development: whether the grain is developed or not (black or white). While having a binary outcome, the response curve of a grain is more subtle and the quantum sensitivity of identical crystals is usually spread according to a normal distribution (See figure 2)[6]. The variance of such a distribution can be modified by changing the parameters mentioned above and will affect the dynamic range that a group of silver halides can register.

When we consider the overall response of a film, we will find a blend of carefully designed crystals of different types and surface areas. Their quantum sensitivity will be crafted and overlapped to expand the dynamic range of a film. Black and White emulsions are usually a blend of two different speed crystals simply called slow and fast crystals. While the change of grain size is rarely visible in the characteristic curve (H&D Curve) of a film, it *can* be detected in the frequency characteristics of the grain (going from big grain only to a mixture of big and small grain in the higher

---

[5] W. F. Berg, *The Photographic Emulsion Layer as a Three-Dimensional Recording Medium*

[6] J.C Dainty and R. Shaw, *Image Science : Principles, Analysis and evaluation of Photographic-Type Imaging Processes, p.88 and 131*

exposures). As a result, noise characteristics, in terms of size and power, will depend on the exposure

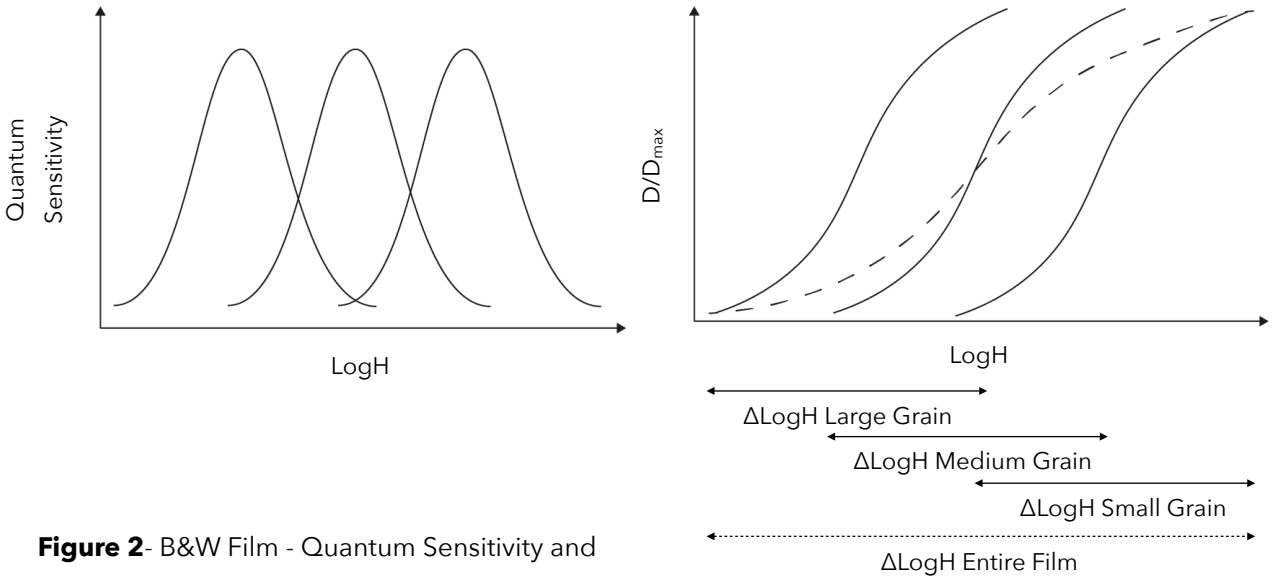

Figure 2- B&W Film - Quantum Sensitivity and Characteristic Curves of single size halides

Even if spectral sensitivity may seem less critical in black and white films, we can note two major film categories. Orthochromatic and panchromatic films are respectively sensitive to short and mid-wavelength (in the visual domain) and sensitive to short, mid and long wavelength in the second (see figure 3). Spectral sensitivity in black and white film is controlled the same way as in color film with sensitizing dyes extending their sensitivity to originally UV and blue wavelengths to longer wavelengths of the spectrum such as green, red and even IR.

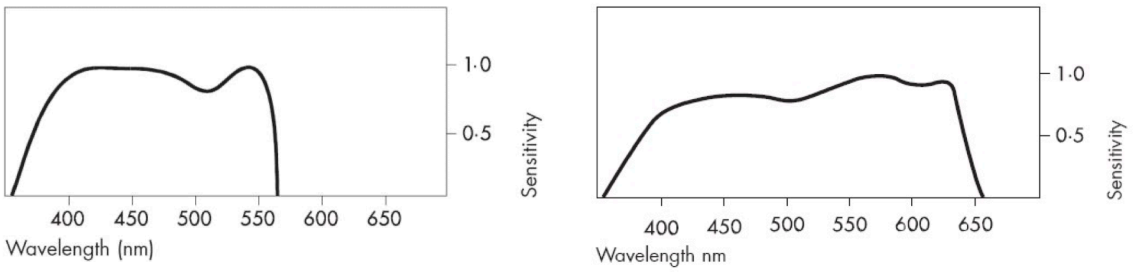

Figure 3 - Ilford Ortho Plus & Ilford HP5 Plus - B&W Spectral Sensitivity - Ilford

Color Negative Film

Chromogenic color films rely on silver halide too but only as an intermediate for the final color image. Silver halides have the physical property to be sensitive to light

which isn't the case of the chemical compounds responsible for the formation of the final dye cloud. Each silver halide is sensitized to a specific band of wavelength thanks to the careful choice of sensitizing dyes. Then color couplers reacting with the side product of the halide development will create dye clouds that will result in the final image. To control carefully the spectral response of a film and how much crosstalk there is between each of its color layers, manufacturers design inner filters used in the film (such as the yellow filter), color sensitizers, intra and inter-layer couplers like DIR (Development Inhibitor Releasing) couplers[7] and even masking dyes[8]. Only being an intermediate in the image creation process, the developed metallic silver is bleached out, leaving the dye clouds the only physical representation of the captured image.

Black and white film final image structure depends on the shape and size of silver halide crystals and develops a representation of the captured image under the form of a metallic silver filament occupying the region originally taken by the halide crystal. On the other hand, color negative film creates an image based on dye clouds unrelated to the shape and size of the silver halide grain that it is associated with. As a result, grain characteristics (mostly spatial frequency characteristics) are not significantly related to the exposure level.

The list of chemical compounds involved in current film lineups aren't known with certainty, but published works from the late 90s and early 2000s give us an overall idea of the technologies and reactions involved in the image creation process.

The level of chemical and physical intricacies and complexity displayed in papers[7] points out that films are evolved chemical technologies sensitive to real world inputs such as temperature, chemistry gradient, light and chemistry crosstalks and photometric considerations such as light scattering.

To acquire relevant data on film and design a simulation modeling grain, rendition of detail, halation and color, we must consider an extended range of exposures. Indeed,

---

[7] *Couplers in Colour Photography—Chemistry and Function Part 3*

[8] R.W.G Hunt, *The Reproduction of Colour*, p.340

we have, thanks to late 70s literature on film, good reasons to believe in a strong dependency between film response and exposure level[9].

1.2 Image Processing

To have a good grasp of image processing, we need to divide image processing into two subcategories: color and spatial processing.
Color processing, as its name suggests, is all about the image color management from white balance to color correction, color space conversion and render intent. Color processing mostly relies on the RGB values of a pixel but rarely takes into account this pixel's neighbors. Not directly related color processes can also be considered part of this category such as tone mapping and every process changing the brightness and contrast of an image.

Spatial processing, on the other hand, is all processes having an influence on the pixel's location in an image. Image filtering is one of the major topics composing spatial processing whether it's done in the spatial, frequency (Fourier) or Wavelet domain. Spatial processing is the field that mostly tackles rendition of detail, noise and compression in an image. Techniques usually rely on analysis and computations based on neighboring pixels and frequency attributes.

[9] J.C Dainty and R. Shaw, *Image Science : Principles, Analysis and evaluation of Photographic-Type Imaging Processes, p.234*

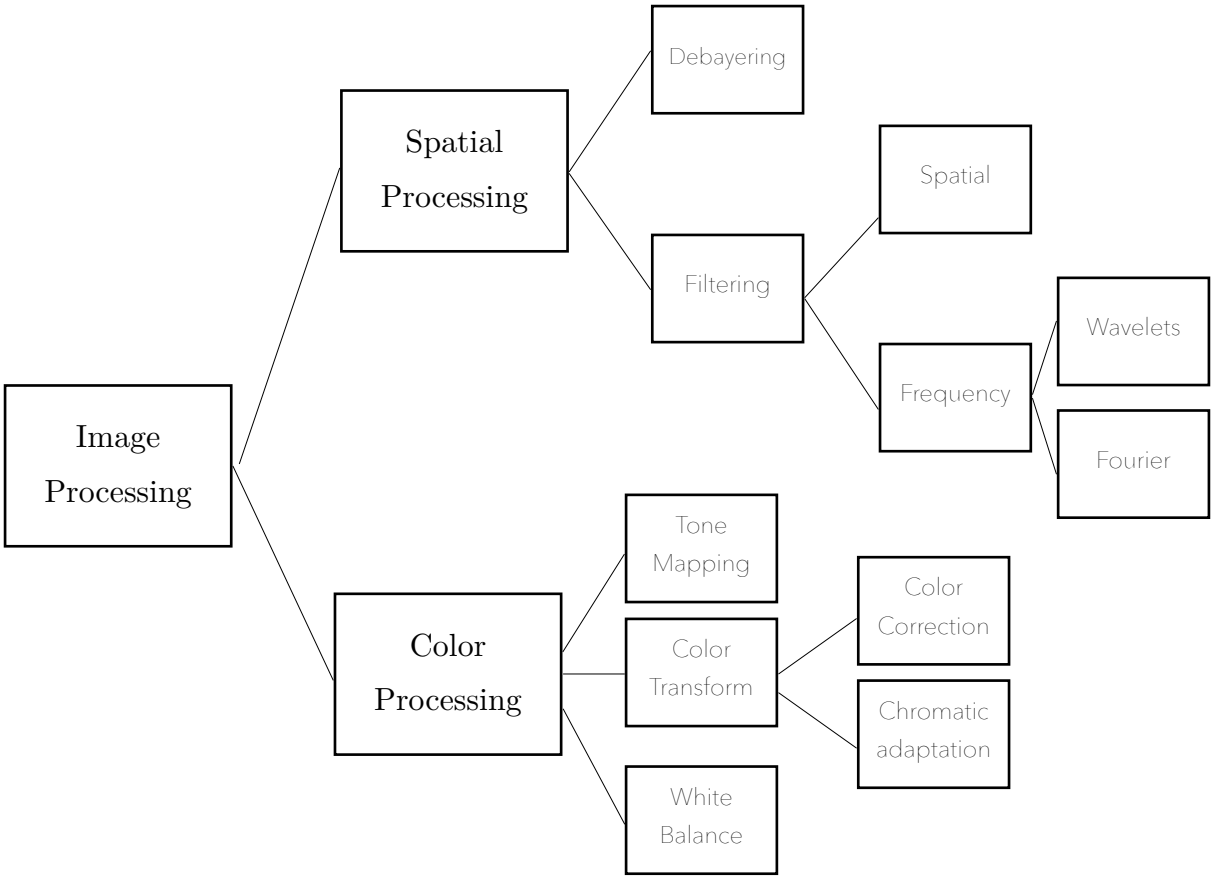

Figure 4 - Overview of the image processing tools

1.2.1 Color Processing

A typical processing pipeline from bayered linear data to screened image is composed of several individual steps relying on color and spatial processing and sometimes both.

Photo and cinema pipelines are slightly different because data is stored differently in both disciplines. The photography industry mostly relies on bayered linear raw data as a starting point of the processing pipeline, then the file is white balanced, debayered, color corrected with a matrix, tone mapped from linear and displayed to the user. In cinema though, while also starting with raw files, the user only has a few steps of the processing pipeline being done. The ungraded signal he receives is scene referred and has not been toned mapped and color transformed for the output display. As a result, the color rendering transform including the tone mapping, the color space transform and the gamma correction (inverse EOTF) for the display is usually contained in an external 3D LUT.

Here is the typical processing pipeline for raw encoded footage before being screened.

White Balance

White balance is one of the simplest processes that can be performed. It consists of multiplying a linear signal by three RGB amplifying factors. The factors have different values depending on the illuminant of the captured scene.

$$RGB_{out}(x,y) = M_{WB} \times RGB_{in}(x,y) \qquad \textbf{Equation 1.1}$$

$$M_{WB} = \begin{bmatrix} R_{gain} & 0 & 0 \\ 0 & G_{gain} & 0 \\ 0 & 0 & B_{gain} \end{bmatrix} \qquad \text{With } G_{gain} = 1 \text{ in most cases}$$

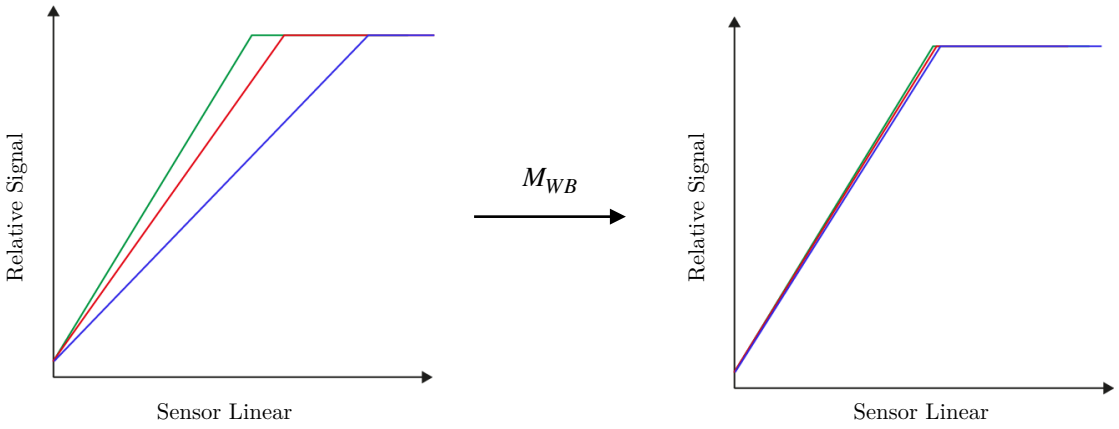

Figure 5 -Signal White Balance

Demosaicing

Demosaicing has been introduced in this document's Glossary under the Debayering definition. Debayering is the demosaicing process for Bayer pattern CFA (Color Filter Array). In the ARRI camera lineup, ADA is the algorithm in charge of this step.

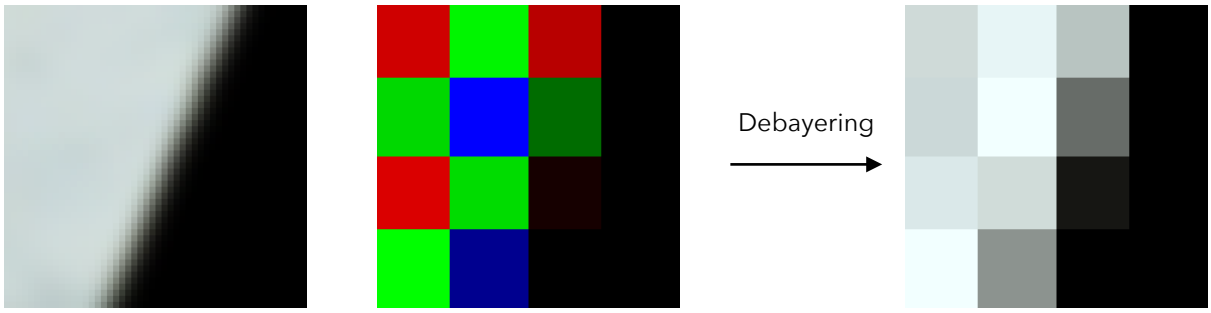

Figure 6 - Debayering schematic

Color Correction

Color Correction is usually handled by a 3x3 matrix. The matrix color correction principle relies on the *hypothesis* that the camera meets the Luther condition which means that a linear transform is sufficient to correct its response. This color correction matrix is illuminant dependent meaning that after white balancing the image, the color correction depends on the captured scene's illuminant.

$$RGB_{out}(x,y) = M_{CC} \times RGB_{in}(x,y) \qquad \textbf{Equation 1.2}$$

$$M_{CC} = \begin{bmatrix} k_{11} & k_{12} & k_{13} \\ k_{21} & k_{22} & k_{23} \\ k_{31} & k_{32} & k_{33} \end{bmatrix}$$

Other nonlinear corrections are possible with higher dimension matrices[10] relying on polynomial expansions that will be discussed later on.

Log encoding

Inspired by film characteristic response, logarithmic encoding color spaces have been designed to reduce the oversampling of highlights in linear signal. Indeed, the last stop before sensor saturation of a captured scene will take half of the linear encoding values. To counteract this effect and get an evenly distributed signal, the signal is

[10] Finlayson, *Color Correction Using Root-Polynomial Regression*

encoded in a logarithmic scale defined by the camera manufacturer. This allows to output files in a 12bits container while still maintaining around 17stops of dynamic range. ARRI has the LogC4 color spaces which are described in their respective white paper[11].

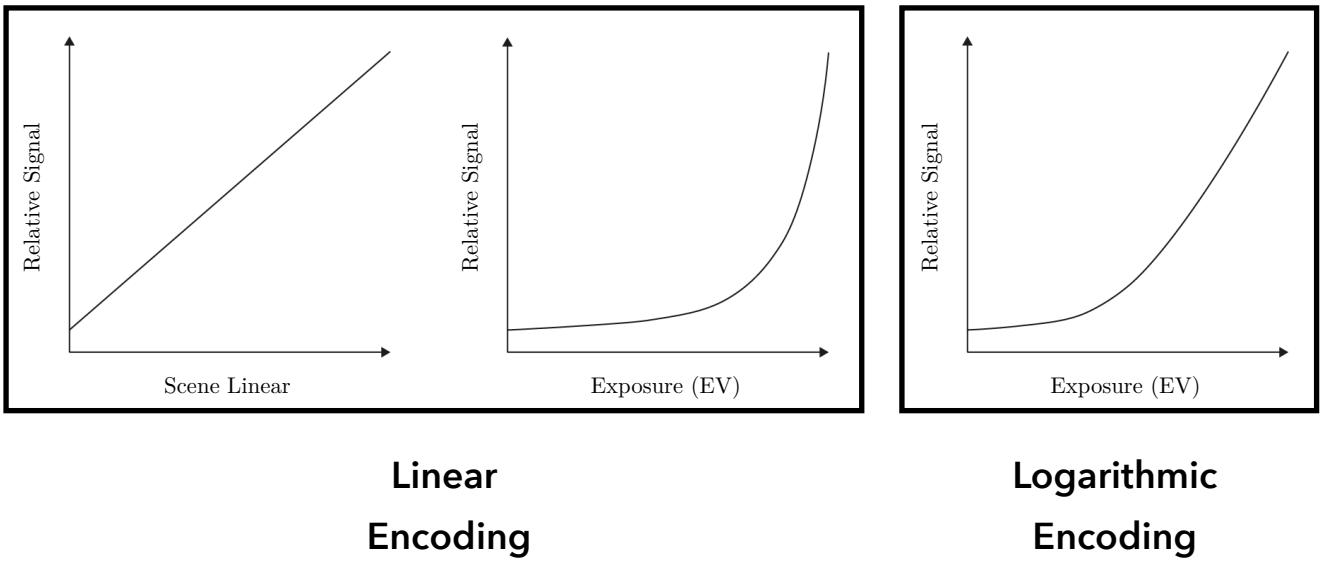

Figure 7 - Logarithmic encoding principle

Tone Mapping

While having a huge advantage in storing efficiently the recorded scene, log spaces are not meeting our visual expectation in terms of contrast stimuli thus needing to be toned mapped. Indeed, because film and log encoding space have much in common, negative films are not the final viewing medium and are printed on analog mediums like print film or paper. These mediums tend to have *S*-shaped sensitometric response, increasing the perceived contrast by crushing blacks and whites around a pivot/midrange point. They are no exact formula as it is empirically driven, but trends like a S-shaped tone mapping are usually used[12].

[11] Harald Brendel, Sean Cooper, ARRI LogC4 Logarithmic Color Space Specification

[12] R.W.G Hunt, *The Reproduction of Colour, p47-67*

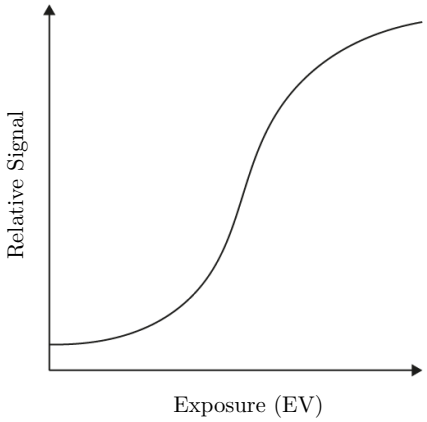

Figure 8 - Common S-Shaped tone mapping curve

Color Space Conversion (Matrix, LUT)

This color space conversion is done from the log color space to the viewing color space. In cinema, one of the widely used color spaces is ITU BT 1886 (Rec.709) which has the same primaries as sRGB. The color space transform is usually based on a matrix computed from a phosphor Matrix (CRT displays) or on the display primaries (more modern displays)[13].

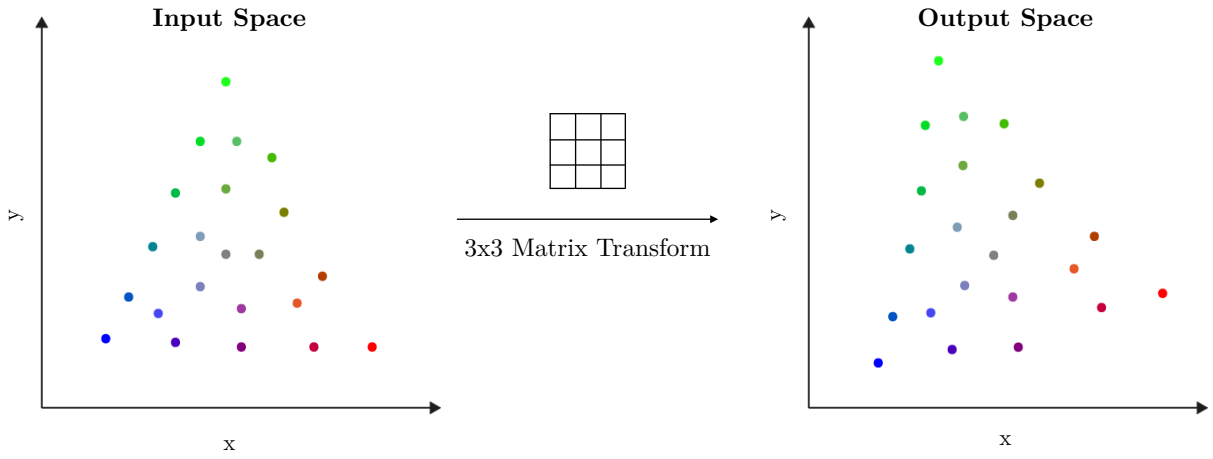

Figure 9 - Color Space transform in a chromaticity diagram

[13] Edward J. Giorgianni, *Digital color management : encoding solutions, p384*

Gamma Correction - Inverse EOTF

Gamma Correction is a transform that is applied before displaying an image on a physical screen. The gamma correction was established based on CRT displays which have an EOTF following a gamma response[14]. While screens have evolved for the past 25 years, the gamma encoding stayed in place even with screens having linear responses. This encoding was kept as a standard as it prevents perceptual under quantization that would occur in linear encoded signal (gamma encoding works on a similar principle to a log encoding).

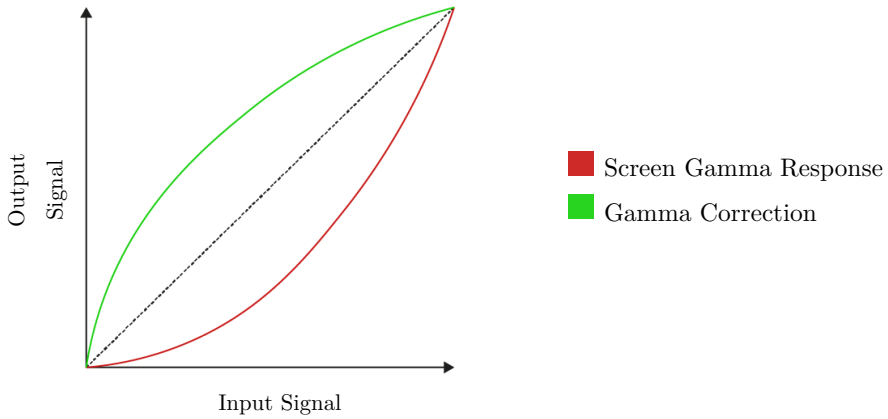

Figure 10 - Gamma encoded curve and its correction

Here is the gamma encoding curve for Rec.709 :

$$S_{Rec709} = \begin{cases} 4.500 S_{linear}, & S_{linear} < 0.018 \\ 1.099 S_{linear}^{0.45} - 0.099, & \text{otherwise} \end{cases}$$ **Equation 1.3**

With S_{Rec709} the encoded signal and S_{Linear} being the scene linear signal

1.2.2 Spatial Processing

In addition to the color processing pipeline described above, spatial processing accounting for denoising, renoising, detail handling and any other upsampling and

[14] R.W.G Hunt, *The Reproduction of Colour, p.50*

downsampling is handled by different types of algorithms based on different processing principles.

To get an overview of this field we need first to introduce image filtering and its two most widely used methods which are Fourier filtering and convolutions

Convolution

Convolution is one of the primary ways to filter images[15]. It relies on the definition of a mathematical two dimensional convolution that has been discretized as in Equation 1.4

$$f'(x,y) = (f * h)(x,y) = \sum_{i=-\frac{d-1}{2}}^{\frac{d-1}{2}} \sum_{j=-\frac{d-1}{2}}^{\frac{d-1}{2}} f(i-n, j-m) \times h(n,m) \qquad \textbf{Equation 1.4}$$

With f' : Filtered image, f : input image and h : square filtering kernel of odd size d.

If the formula is intimidating the visual representation of a convolution is simple and can be explained by this schematic.

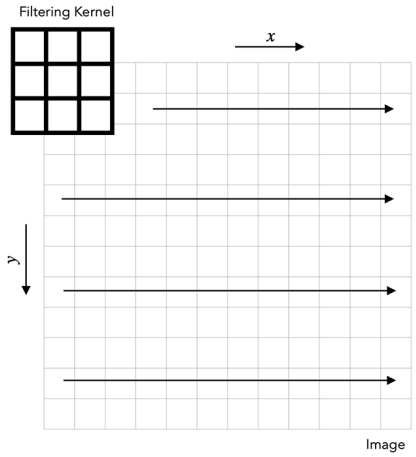

Figure 11 - Convolution principle

[15] J.C Dainty and R. Shaw, *Image Science : Principles, Analysis and evaluation of Photographic-Type Imaging Processes. p.190-231*

The filtered image will then receive the computed value which is the sum of the multiplications of the input image values and the filter kernel. Here are some examples of 3x3 kernels

0	0	0
0	1	0
0	0	0

Identity Filtering

$$\frac{1}{9} \times \begin{bmatrix} 1 & 1 & 1 \\ 1 & 1 & 1 \\ 1 & 1 & 1 \end{bmatrix}$$

Box Blur

$$\frac{1}{16} \times \begin{bmatrix} 1 & 2 & 1 \\ 2 & 4 & 2 \\ 1 & 2 & 1 \end{bmatrix}$$

Gaussian Blur

0	-1	0
-1	5	-1
0	-1	0

Sharpening Filter

Fourier Filtering

Fourier Filtering[16] is an equivalent of convolution in spatial domain but transposed to Frequency domain. The image is decomposed in frequency levels based on a Fourier decomposition.

Discrete Fourier Transform

$$DFT(x(n,m)) = \frac{1}{N \times M} \sum_{n=0}^{N-1} \sum_{m=0}^{M-1} x(n,m) e^{-2i\pi(\frac{un}{N} + \frac{vm}{M})} \qquad \textbf{Equation 1.5}$$

Discrete Inverse Fourier Transform

$$DFT^{-1}(X(n,m)) = \frac{1}{N \times M} \sum_{n=0}^{N-1} \sum_{m=0}^{M-1} X(n,m) e^{2i\pi(\frac{un}{N} + \frac{vm}{M})} \qquad \textbf{Equation 1.6}$$

One can note that the Fourier Transform of an image is a complex number composed of a real and imaginary part.

NB : Discrete Fourier Transforms DFT will be noted $\mathscr{F}$ in the rest of the thesis for simplification purposes.

The equation defining the relationship between convolution and Fourier filtering is globally defined as the following

$$(f * h)(x,y) = \mathscr{F}^{-1}(\mathscr{F}(f) \times \mathscr{F}(h))(x,y) \qquad \textbf{Equation 1.7}$$

---

[16] J.C Dainty and R. Shaw, *Image Science : Principles, Analysis and evaluation of Photographic-Type Imaging Processes. p.190-231*

1.2.3 Spatial metrics and concepts

As one can imagine, Texture is mostly about the physical appearance of an image (and not really about its colors), it heavily relies on spatial processing. Fourier and spatial domains can be chosen to picture measures and behaviors in a more meaningful matter. In the next section, we will try to understand the link between filtering with convolution and Modulation Transfer Functions. We will also introduce the link between noise filtering and Noise Power Spectra.

Modulation Transfer Function[17]

Computing the Modulation Transfer Fonction of a given system is meant to test how well frequencies are transmitted through our opto-electrical system. Similar to sound which is defined with temporal frequencies, photography is sampling space as a set of spatial frequencies. Keeping the sound analogy, when we want to assess the frequency response of a given system, we send a white noise containing all frequencies with equal energy through our sound system. When considering photography and opto-electrical systems, objects containing all frequencies at equal energy are small points, thin lines and sharp edges. As a consequence, to get an idea of the frequency response of our imaging system, we need to image one of these objects through it. When doing an MTF, we have to be aware that we are measuring the entire imaging system with its lens, OLPF, optical stack and image processing (debayering, spatial filtering …).
Here is an example of the opto-chemical-electrical elements that influence the frequency response/MTF of the film imaging pipeline.

[17] J.C Dainty and R. Shaw, *Image Science : Principles, Analysis and evaluation of Photographic-Type Imaging Processes, p.232-275*

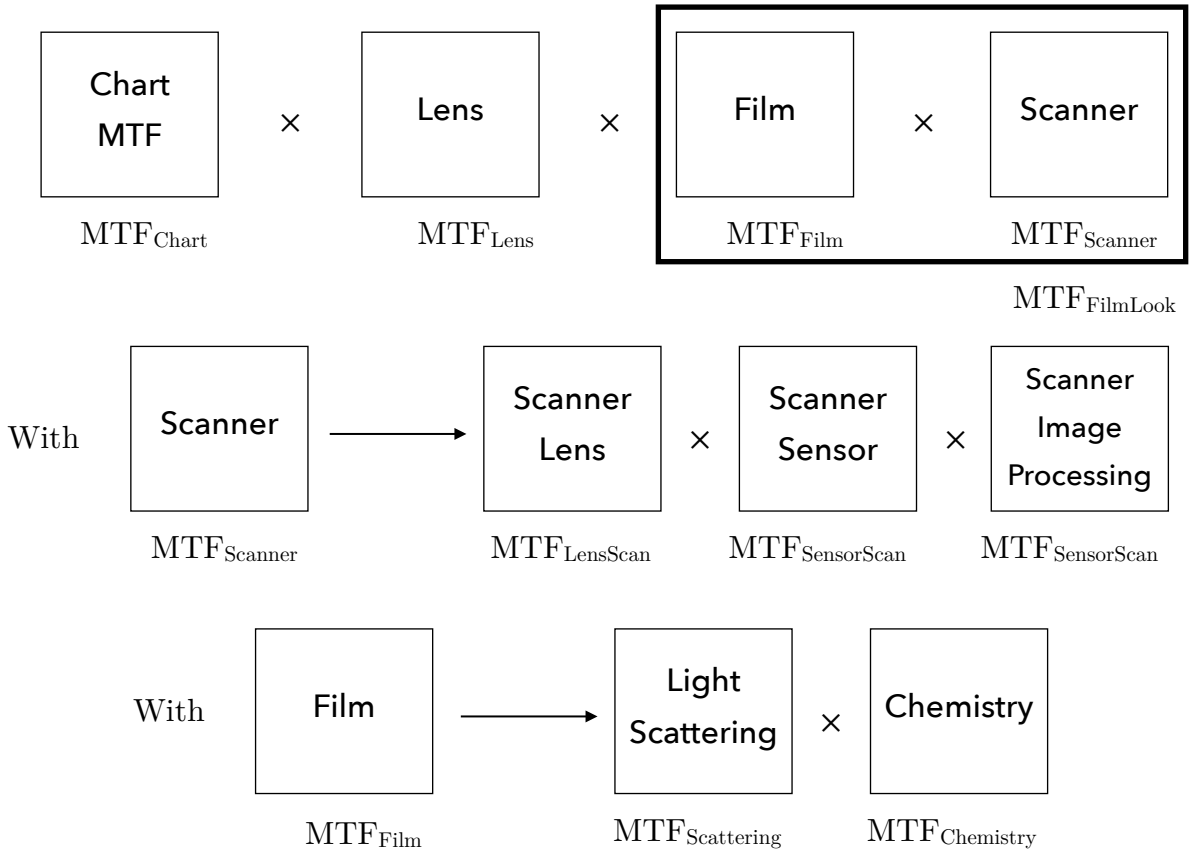

Figure 12 - MTF product principle

To introduce the shared principles between convolution kernels and MTF, we can illustrate this with the following examples.

There are two ways to retrieve the frequency response or MTF of our system. One is computing the frequency response of our filtering kernel by padding it to the appropriate resolution and Fourier Transform it, the other is considering the edge spread function of a filtered edge, derive it and compute the Fourier Transform of this derivation.

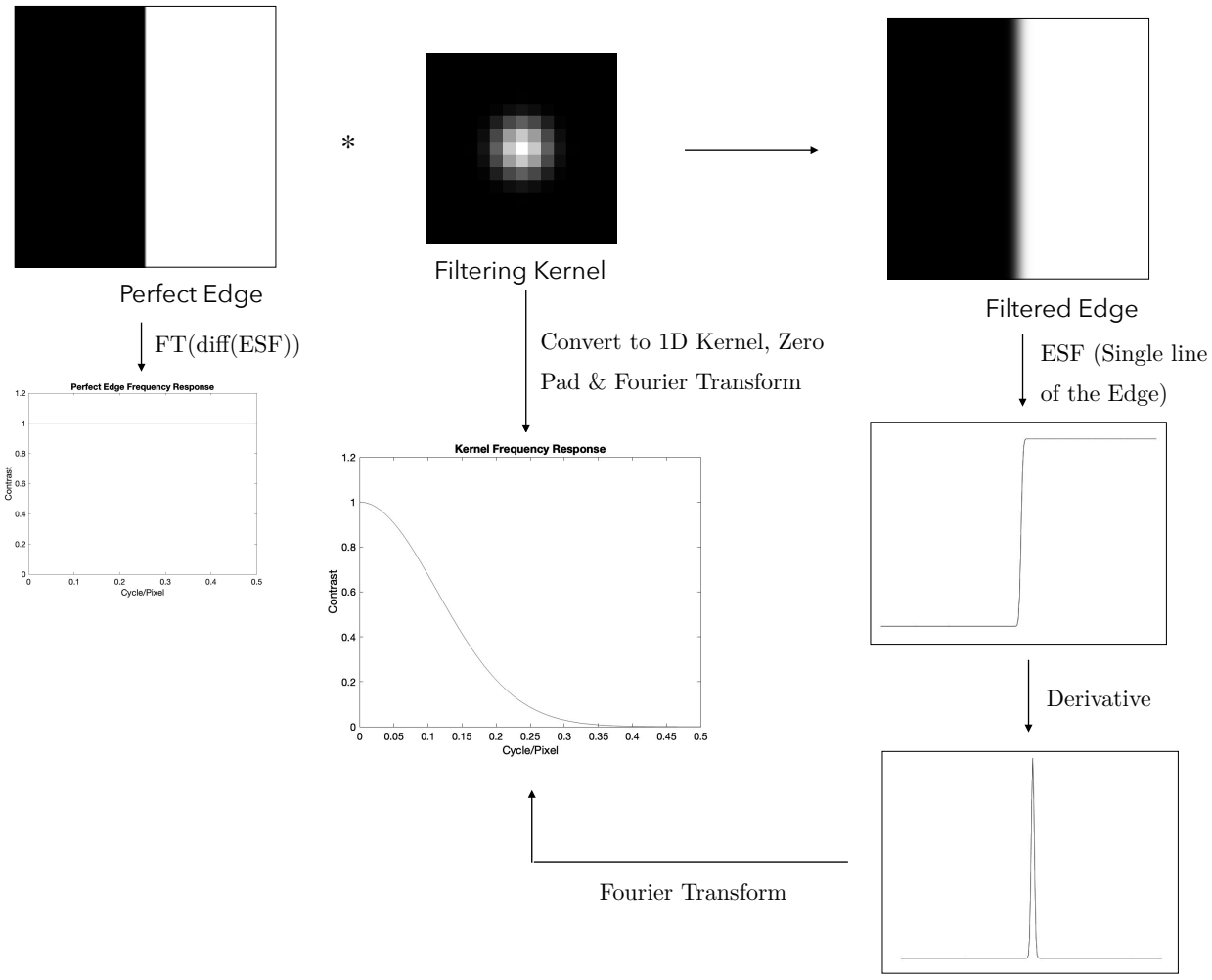

Figure 12 - MTF computation principle

NB : In Figure 12, 'Fourier Transform' stands for the Fourier Transform's magnitude.

Noise Power Spectra[18]

With a similar principle as MTF, Noise Power Spectra gives information of the frequency characteristic of the analyzed noise. Similar to a sharp edge or a thin line containing all frequencies at equal power, White Noise or unfiltered noise contains all frequencies at equal power.

To know the frequency response also called spatial correlation of a given noise we have two different ways of doing so. One way is, as presented in the MTF section,

[18] J.C Dainty and R. Shaw, *Image Science : Principles, Analysis and evaluation of Photographic-Type Imaging Processes, p.222, NPS referenced as Wiener Spectrum*

taking a padded kernel and computing its Fourier Transform to retrieve its spatial correlation.

The second one is computing the AutoCorrelation matrix of the filtered noise and taking the Fourier Transform of this matrix. To be a bit more specific, the frequency response can be fully retrieved when the AutoCorrelation is squared before being Fourier Transformed or the Fourier Transform is square rooted.

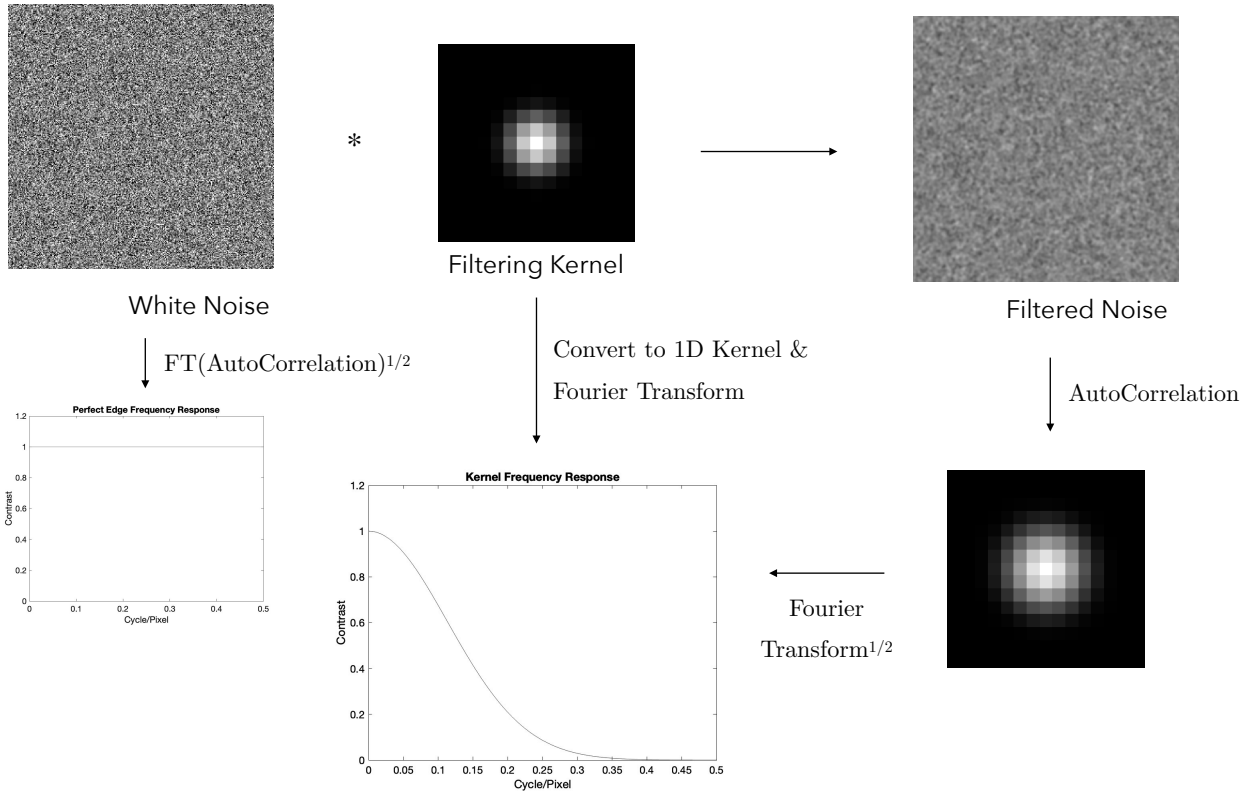

Figure 13 – pseudo NPS computation principle

1.3 Current texture synthesis knowledge

Grain

Grain is the most researched of the 3 ingredients identified as film texture. We can even identify several methods that claim to achieve film grain from the simplest scanned grain plates up to full physic and statistic-based simulations[19].

Film grain is the essence of the material attribute of film as it relies on physical crystals to capture light. Furthermore, film grain is both modified by the thickness of the film base and the layering of the film-sensitive emulsion. As the final film data is scanned by a film scanner or duplicated by a contact print device, the optical characteristics of the lens and/or the sensor are concatenated into the film itself.

Signal Correlation

Film being a light capturing device, the medium is inherently affected by photon shot noise. This shot noise is inherent to light and follows a Poisson distribution. At high enough signals, this noise usually follows a Gaussian distribution[20]. Photon shot noise is indeed signal correlated and increases linearly with exposure.

Furthermore, crystal halides themselves have an inherent noise built into their reaction to light. Also following a Poisson distribution at low intensity, it can be approximated by a Gaussian distribution at higher exposures. Film noise increases according to a square-rooted function (B&W film) in a log domain (Optical Density)[21].

Spatial Correlation

Silver halides once reduced by the developer form tiny spheres or filaments of metallic silver. It's worth noting at this point that even if the size of the sphere or filament is correlated to the size of the silver halide (in terms of boundary), many other parameters influence the size and shape of resulting silvers like chemistry

---

[19] A Newson, Julie Delon, B Galerne. *A Stochastic Film Grain Model for Resolution-Independent Rendering.*

[20] Andrews, Harry C, *Digital image restoration, p.21*

[21] ibid.

diffusion, development agitation and composition of the developing bath. Furthermore, for color films, the final image elementary structure is even more remotely correlated to its halide due to the greater complexity involved in the creation of dye clouds and thus in the resulting image. As individually as resulting silver filament/dye clouds can be described, spatial correlation caused by the neighboring effect of development due to local gradient of chemistry concentration as well as electron exchanges between those sites is observed.

Independently of the film and the correlation brought by exposure and chemistry, the device used to print or scan the film will now shape the output spatial correlation of the grain. Its lens and/or sensor frequency response will end up being concatenated into the film grain spatial correlation. Last but not least, still taking the scanning/ duplicating device into account, the geometry of the light source used by such device to illuminate the film is of great importance. Indeed, using a condensed light source will bring Callier effect[22] thus increasing the grain sharpness and power whereas using a diffuse light source will soften (or render it as is) the grain while lowering its power at the same time.

Spatial correlation of film grain will be evaluated in scanned images resulting in a quantization of the spatial pitch involved in the measurements.

Color Correlation

Color correlation in film grain can be explained by the structure of the film and more specifically how it is arranged into layers stacked one upon another. As a consequence, when the film is exposed to light, layers on top of the optical stack will have an impact on layers beneath it (mostly due to light scattering of silver halide crystals and chemistry diffusion). Moreover, and probably the most impactful of the two, once developed, scanned or duplicated, a film will be read with a light shining through its optical stack and thus revealing shadowing and occlude effects between different layers. All combined, these effects will create a correlated noise signal between each color layer on a spatio-color level.

[22] R.W.G Hunt, *The Reproduction of Colour, p.222*

To summarize, film grain is correlated on three different levels which need to be adequately measured and replicated to get a proper grain synthesis. One of these correlations will highly depend on image content (signal correlation) while the other two will mostly depend on the physical structure of the the film itself.

Rendition of detail

Rendition of details is an aspect of film emulation that remains mostly not tackled in currently available synthesis. We noticed that measuring film MTF was challenging due to the lack of dedicated tools to measure such characteristics and the high noise level encountered in a film. Aside from apparent blur filtering that has to be manually dialed in by the user, there is no trace of actual filtering based on such measurement. Rendition of detail will be considered as a combination of a physical and chemical effect: light scattering in the emulsion causing blurriness and chemical gradient[23] causing adjacency effect and thus sharpening.

Halation

Halation is another characteristic without significant research or documentation. The principles involved in the effect are somewhat known but rarely clearly defined and graspable. Existing tools emulating halation rely on user input thus based user's depiction of halation but no objective measurements. As a result, this flexibility can lead to unrealistic results when it comes to emulating faithfully a given film. Parameters like strength, threshold, size, and fall-off are relevant for aesthetic choices but not faithful to a given filmstock.

1.4 Digital Camera - ARRI Alexa 35

The Alexa 35 is an ARRI camera released in 2022 and introduced a new color processing pipeline called REVEAL, a new color space (AWG4) and encoding curve (LogC4) as well as a new feature called Texture allowing cinematographers to control the spatial attributes of their footage even further by changing noise and sharpness.

---

[23] J.C Dainty and R. Shaw, *Image Science : Principles, Analysis and evaluation of Photographic-Type Imaging Processes, p.237-238*

The Alexa 35 features a 4,6K 3:2 sensor and has a great dynamic range reaching a staggering 17 stops. ARRI Signature Primes are the lenses that were preferred to acquire data with the Alexa 35.
The processing pipeline used in the camera is similar to the one described in the Background section.

1.5 Film Scanner - ARRISCANXT

To scan the film we exposed, we used an ARRISCANXT. It is ARRI's second generation of scanners. It is equipped to mechanically advance the film through a 35mm or 16mm gate. The sensor is a monochromatic Alev3 sensor equipped with a Zeiss macro lens. Because of the monochromatic sensor, the illumination is composed of 3 sets of LEDs covering spectrally ranges of red, green and blue. To get a highly homogenized illuminated surface, the light source is diffused with an integration sphere. As the Alev3 sensor is only 3.4K, the scanner can perform a half pixel shift to get double the native scanner definition (6.8K) at the cost of reduced scanning speed.

As with most scanners, or imaging devices, its opto-electric response characterization is key to get consistent and reproducible results. The ARRISCANXT is no different as it is calibrated with a given set of filmstocks (Fujifilm and Kodak) to get appropriate and defined results in terms of colorimetry and tonal reproduction.
Furthermore, when no film is loaded, the scanner is calibrated with a sensor linearization and flat field correction.
A film calibration consisting of a film base+fog subtraction is performed by adjusting the RGB channel level of the LED illumination.

As mentioned above, color informations are obtained from a set of RGB LEDs. Even if the LEDs spectral emission can't be displayed in this thesis, we can hypothesize with confidence fairly narrow band RGB LEDs that are close to the maximum densities of common negative film dye sets. This principle of measurement at peak

densities in the cyan, magenta and yellow layers is also the one adopted by the sensitometric standard Status M as well as SMPTE Printing Densities.
Yet, while the illumination RGB LED emission spectrum approaches the spectral response of Status M or Printing Densities, they are not exactly the same. As a result, to correct properly the scans coming out of the scanner, color correction matrices are computed based on film measurements. Each combination of code values was then spectrally measured and integrated with the 3 most common measuring standards which are StatusM, Printing Densities and APD[24] (ACES Printing Densities). With these integrated values, a color correction based on an 3x3 matrix is optimized to reduce the color discrepancies between the input (RGBScan) and output (Integrated StatusM, Printing Densities or APD). This color correction occurs in scanning density (log domain with a similar encoding as Cineon) encoded domain.

ADX10[25] while having a different definition (based on APD, see Equations 1.10) has shared grounds with Cineon encoding. Both of them are logarithmic encoding systems using the definition of optical densities. The sensor captures linear data from the negative film which corresponds to the film transmittance. Optical Density on the other hand is defined as in equation 1.8. The density encoding for the ARRISCANXT is based on Cineon and is defined as in equation 1.9.

$$D = log(O) = -log(T) \text{ with } O = \frac{1}{T} \qquad \textbf{Equation 1.8}$$

Density Encoding of raw ARRISCANXT footage

For $C \in [R, G, B]$ and $[R, G, B] \in [0,1]$

$$\boxed{Cineon_C = -log_{10}\left[MAX[C,0.00001] \times CinGain + Offset\right]} \qquad \textbf{Equation 1.9}$$

[24] SMPTE, SMPTE ST 2065-2:2020, *Academy Printing Density (APD) - Spectral Responsivities, Reference Measurement Device and Spectral Calculation*

[25] SMPTE, SMPTE ST 2065-3:2020, *Academy Density Exchange Encoding (ADX) Encoding Academy Printing Density (APD) Values*

$$\text{Where } CinGain = \frac{GainVar}{500.0} \quad , \quad Offset = \frac{BaseVar + log_{10}\left(k \times GainVar\right)}{1024}$$

ADX Definition as in SMPTE Standard **Equations 1.10**

$$ADX_{Red} = MAX[0,MIN[1023,ROUND[1.00 \times (APD_R - APD_{RDmin}) \times 500 + 95]]]$$

$$ADX_{Green} = MAX[0,MIN[1023,ROUND[0.92 \times (APD_G - APD_{GDmin}) \times 500 + 95]]]$$

$$ADX_{Blue} = MAX[0,MIN[1023,ROUND[0.95 \times (APD_B - APD_{BDmin}) \times 500 + 95]]]$$

$$\text{Where } APD_C = -log_{10}\left[\frac{1}{\prod_{sum,c}} \sum_{\lambda} \prod_{\lambda,c} \times T_\lambda\right] \text{ and } C \in [R,G,B]$$

T_λ : Spectral Transmittance of the measured sample (film) at a given wavelength

$\prod_{\lambda,c}$: Spectral response of $\prod_{APD}$ per channel (RGB)

2 - Dataset acquisition

This section describes the protocols used to acquire the footage needed to extract data from analog film.
Each texture characteristic needs a specific testing setup to be extracted from the captured footage. Furthermore, those characteristics are tightly coupled to specific encoding curves and color spaces to be properly defined.

2.1 Sensitometry

Film characteristics' dependency on exposure has been one of the main hypotheses. Some film attributes like color rendition which were studied in a preliminary work before the thesis, already showed non linear behaviors and were tied to exposure level. Furthermore, as explained in section 1.3, all imaging devices are victims of photon shot noise. As a result, we decided to acquire data with this constraint taken into account. Each dataset contained exposure ramps of 18 stops with a repartition of the top above and below 18% gray based on the ISO standard.
The ISO standard[26] determining color negative film sensitivity called for the mean of the green and slowest layer sensitivity based on their logH as in Equation 2.1 (H being the illumination in lux.s). Those logH are the illumination necessary to generate 0.15D above Dmin. To meet the ISO standard, the film is supposed to reach a gamma of 0.6.

$$log_{10}H_m = \frac{log_{10}H_G + log_{10}H_{SlowestLayer}}{2} \qquad \textbf{Equation 2.1}$$

$$S = \frac{\sqrt{2}}{H_m}$$

[26] ISO 5800:1987, Photography, Colour negative films for still photography Determination of ISO speed

While getting the speed point gives a lower boundary idea for our film bracketing, we usually expose scenes based on 18% gray. Furthermore, we realize while studying Sekonic or Minolta lightmeter's equations that 18% gray is set to be around $3_{2/3}$ EV above the speed point.

With this information in mind, we can expose our films with an 18 stops bracketing range to measure the film response from noise floor to saturation point. 18 stops was chosen because it covers the Alexa 35 range and also because it is half of a 36 frames 135 film roll. We decided to put 6 stops under 18% Gray and 11 above it.

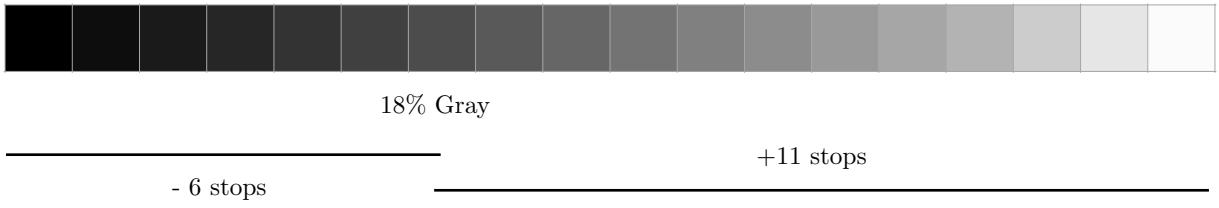

Figure 14 - Exposure range and stop repartition for film

2.1.1 Linearizing film

Linearizing film was a prerequisite to all analysis steps in one way or another. For example, linearizing for grain analysis seemed not required at first glance, but because of the dependency of grain appearance depending on the color space, we linearized the film to do a color space transform to LogC4. For RoD and Halation analysis, the signal must be linearized before computing the film's MTF.

With the recommended gamma of 0.6, knowing that the speed point is defined at 0.15D above base+fog, and with 18% gray around $3_{2/3}$ stops above speed point, 18% gray should correspond to a density of around 0.8D.
With more precision and relying on a norm, while checking Kodak LAD (Laboratory Aim Density) given in their *Digital Recorder Calibration*[27] the 18% gray target is

[27] KODAK Publication No. H-387, *KODAK Digital LAD Test Image, User's Guide and Digital Recorder Calibration and Aims,*

given for a 445 Cineon value (in 10bits). On negative film (50D in Kodak's document), the yielded density above base fog is around 0.7D depending on the layer (in StatusM) but exactly 0.7D in Printing Densities. Furthermore, in ACES's ADXToAP0 CTL file, mid-gray is also rated at 0.7D[28]. This will be our reference to adjust gray point in our linearizing algorithm.

NB : 0.7D is not the measure we want in our process which is based on relative ADX10 values. Gray point will be defined as

$$GP = \frac{0.7D * CinGain + 95}{1023} \qquad \textbf{Equation 2.2}$$

2.1.2 Light Sensitive Surface Exposure

Exposing a light sensitive surface whether it's photographic film or sensor is challenging. In film, light sensitivity is described as the amount of light required to produce a target density above film base and fog. ARRI uses an EI scale (directly based on the ISO standard sensitivity scale[29]) defined by the 18% gray value. As the sensitivity increases, the repartition of above and below 18% gray stops is shifted (The higher the sensitivity, the higher the number of highlight stops available)[30]. It implies that there is a single hardware sensitivity and that additional sensitivities are created changing the log encoding curve based on the software EI user (or metadata) input.

2.2 Grain Plates (Flat Fields)

Grain in film can be measured when a uniformly lit surface with a properly balanced illumination is photographed. To measure the proper spatial correlation of the grain,

---

[28] ACES ADXToAP0 CTL file on GitHub

[29] ISO 12232:2019, Photography - Digital still cameras - Determination of exposure index, ISO speed ratings, standard output sensitivity, and recommended exposure index

[30] ARRI, ALEXA 35 *Software Update Package 1.2 User Manual*, p.41

the surface that is used to create these grain plates shall also be textureless. Given these constraints, an integration sphere is a great candidate for the task. As grain characteristics vary with exposure, we will take multiple frames across an 18-stop exposure range.
As it will be explained in section 3, grain plates have to be carefully converted to the right color space before analysis as their characteristics drastically change with space conversions.

2.3 Slanted Slit

The slanted slit method can be seen as a double slanted edge method[31]. This allows to get double the edge length for a single frame. This helps tremendously as film is really noisy which leads to inaccurate or even unusable MTF. The slanted edge allows to measure the rendition of detail and halation of a given film.

Even if the slanted edge is commonly used in digital photography to measure lenses MTF the method is rarely used in film and even less used to characterize halation. With basic MTF principles we can deconvolve the lens MTF from the concatenated Film MTF and Lens MTF we get out of the ARRISCAN (Scanner MTF is considered to be part of the film texture). Yet, the MTF doesn't account for lens flare and other optical aberrations that will be present in the measurement.
As a result, we decided to try and get a slanted edge without any lens in front of the film and just get the shadow of a razor blade directly against the film. Even with pre-tests displaying diffraction issues by the razor blade, we thought that they were visible only because of the gap between the razor blade and the sensor (being roughly 5cm apart from one another). Yet, even being nearly directly in contact with the film (around 100µm away corresponding to half a razorblades thickness) still showed a huge diffraction effect not suited to precisely measure the MTF of film. Furthermore, simulation tests (see Figure 15) based on the knife edge diffraction gave us results that completely disqualified the method to measure MTF (Overshooting

[31] Estribeau, Magali, et Pierre Magnan. *Fast MTF Measurement of CMOS Imagers Using ISO 12333 Slanted-Edge Methodology*

on the bright side of the edge and «flare» polluting the darker side of the edge (see additionally Appendix 1)).

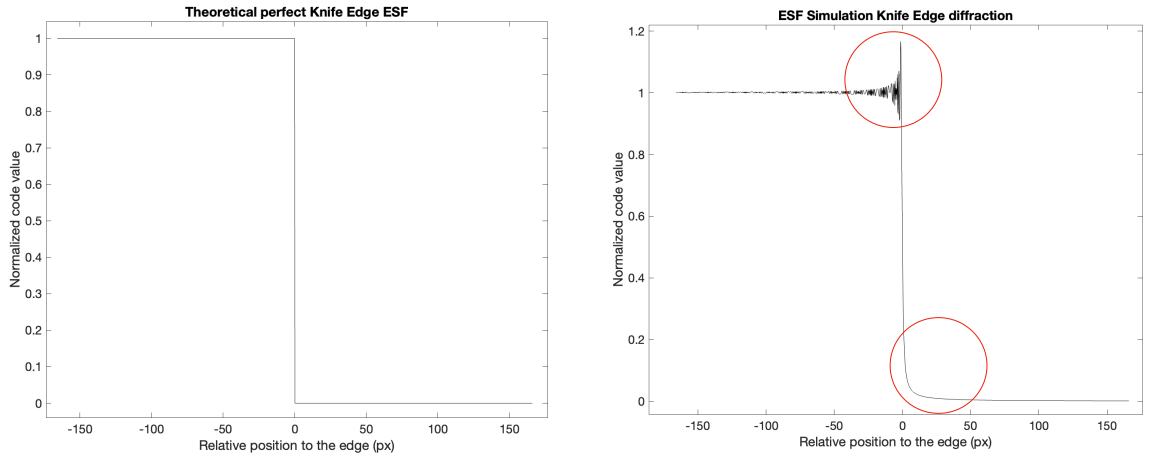

Figure 15 - Theoretical ESF and Knife edge diffraction simulation

As the razor blade was not successful, we decided to use a regular method with a system relying on a lens and a slanted slit chart. As mentioned above, this method could only bring us so far as flares and aberrations would become visible in higher exposures. The measurement method was considered sufficient and the optical aberrations non-disturbing.

To get a system of cameras that could both be digital and analog, we decided to use Nikon still cameras as they did not change their lens mount in the 2000's when they switched to digital cameras.

Because getting critical focus with an analog camera is difficult, we decided to use the digital camera as a focusing tool. Because we were aware of potential focus discrepancies between the two mediums, we started to asses what position difference there was between analog and digital. We locked our lens's focus ring to 70cm and decided to focus the camera by moving it on a scaled optical bench. A position bracketing was done both with the digital and analog camera (loaded with black and white film). To assess critical focus, captured slanted slits were processed to get the MTF out of them. Plots showing MTF50 (computed on average RGB channel) depending on the position relative to the chart were made and allowed us to assess the distance separating the critical focus position in both mediums (See Figure 16).

At that stage, MTFs were computed with the sfrmat5 program which relies relying on edge detection. This gave us noisy but reliable results for the focus assessment of the analog camera. You will find all MTF plots for both mediums in Appendix 2

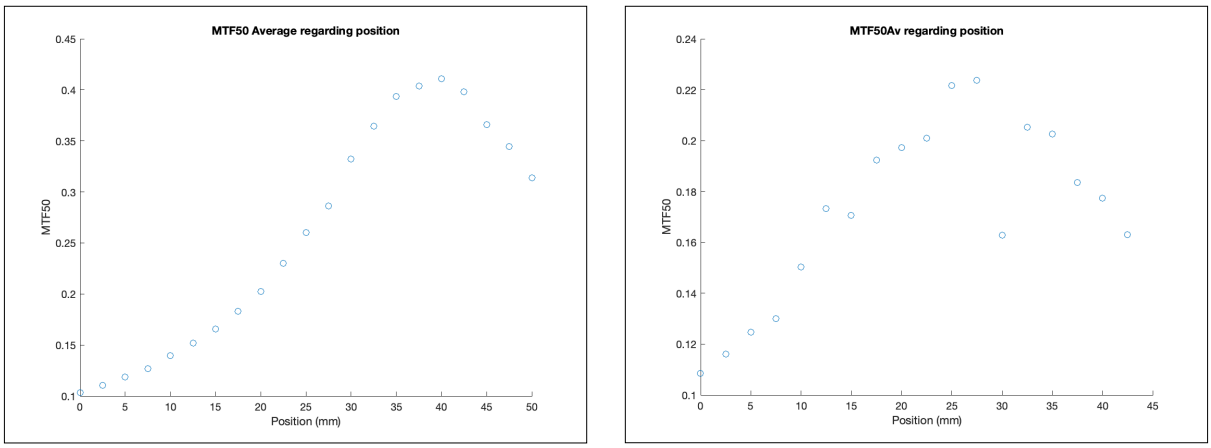

Figure 16 - MTF50 regarding position - Digital and Film

The digital camera was used to position properly the mounting plate on the optical bench and then, the offset distance (evaluated at 15mm) computed the day before was applied to the film camera. The slit chart was shot with an 18 stops range of one stop increments to get RoD and Halation information throughout the exposure range.

The films were developed in an ECN-2 processing chain and scanned with an ARRISCANXT. The scans are 4K downsampled 6K footage, filtered by the OCN2 digital filter set to 0 blur and 0 sharpness. The scanner offers the ability to get not downsampled and not filtered footage but it has been chosen to stick with what users might use in a regular film scanning. Furthermore, it has been observed that the standard deviation of the finest grain structures exceeds 0.5 pixels telling us that we can retrieve any additional information from the film.

Additionally and to put things into perspective, at a 4K resolution for 35mm film (24mm wide), the scanner yields a pixel pitch of 6e-3mm/px yielding a resolution of 166.6px/mm which roughly converts to 4200dpi.

Once the films are scanned, the files are loaded into Matlab, and color space is converted to LogC4 according to ACES's ADX10 pipeline.

2.4 Assessment Data

The assessment data was acquired to compare Kodak Vision 3 filmstocks with the texture and color emulation applied to Alexa 35's footage. To get a good grasp of what's going on with the emulation, we acquired data ranging from portraits of people with various skin tones, color scenes with synthetic and natural objects up to outdoor images of green and earthy tones.

3 - Color reproduction

3.1 ACES film color management

Introduced in section 1.5, the ACES film encoding system is based on ADX10. ADX10 is a rigorously defined encoding space directly depending on APD characteristics[32]. The color processing pipeline introduced by ACES to convert ADX10 to ACES AP0 is presented in a CTL publicly available on their Github[33]. The pipeline is built around various processing steps composed of matrix transform and linearization LUT.

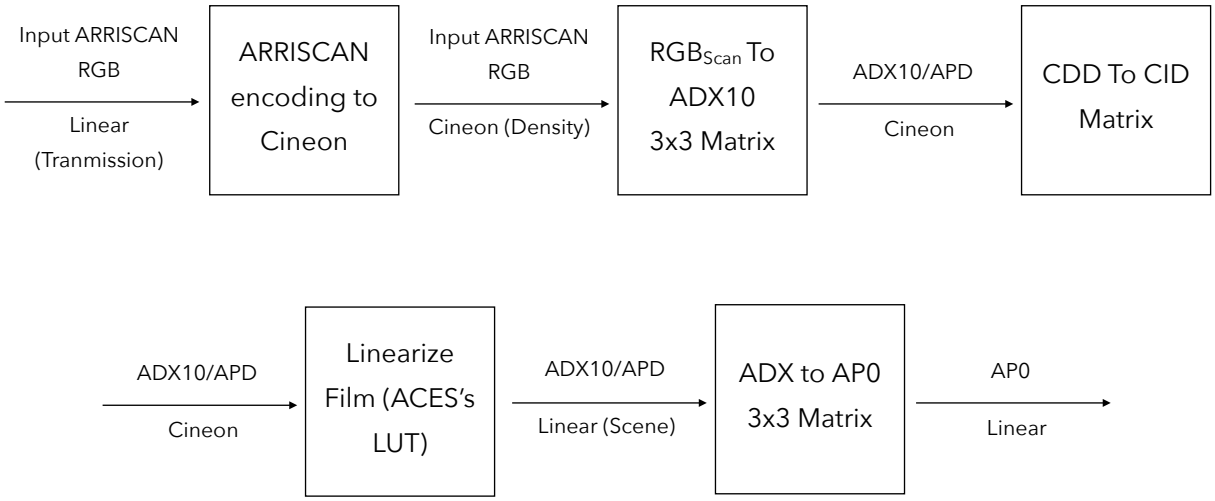

Figure 17 - ACES Pipeline - ADX10ToAP0

This ACES color processing pipeline reduces nonlinearity observable in film and improves our upcoming optimization to compute a matrix transform between Alexa35 and Film. Moreover, as we measured a more specific characteristic curve for

[32] SMPTE, SMPTE ST 2065-3:2020, *Academy Density Exchange Encoding (ADX) Encoding Academy Printing Density (APD) Values*

[33] ACES's ADXToAP0 CTL file on GitHub

each of our films, we can perform the linearizing step with our own LUT instead of the generic ACES provided one.
To complete the color space transformation to LogC4/AWG4, we continue the color space transform according to this processing pipeline :

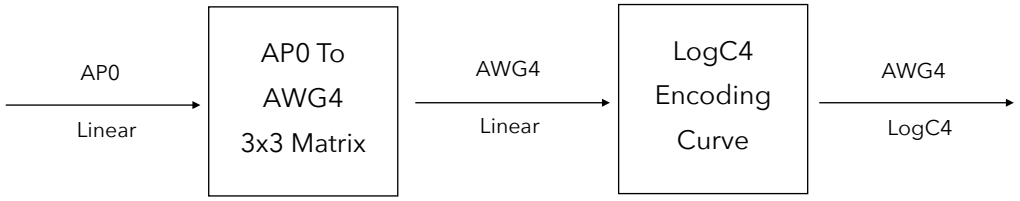

Figure 18 - Color processing- AP0ToLogC4

All analyses are performed in AWG4/LogC4 domain as we need to evaluate the grain, RoD and halation characteristics in the synthesis domain. Therefore, scans are processed through the just presented color pipeline.
However, even if we adapted the processing pipeline with a data-driven linearization LUT, the color space matrix transform between ADX10 and AP0 remains generic. To get a more accurate correction, we can acquire a Color Checker SG at different exposures with both mediums (film and digital) and compute a 3x3 color correction matrix. This process will be further detailed in the following sections.

3.2 Data Extraction

To drive our optimization algorithm for the color correction between Alexa35 and film, we need to extract patches that have been exposed to the same level of light. To take into account the remaining nonlinearities (regarding exposure) of film even after the CDD To CID matrix correction, we decided to optimize our matrix for several exposures. The correction will be optimized on a 6 stops bracketed range (±3EV around 18% Gray).
Alexa 35 footage was acquired with a cinema lens graduated with Tstops whereas the film data was captured with a photographic lens graduated in Fstops. Therefore, transmission is not taken into account by the photographic lens leading to errors in the frame matching. We need to find the closest match exposure between film and

digital with a simple 18% gray analysis. Once done, the Color Checker SG can be extracted patch by patch for every exposure of both digital and film.

3.3 Color Correction

The equation we are trying to solve to match our digital camera to our film can be presented as

$$B = M_{CC} \times A \qquad \textbf{Equation 3.1}$$

$$\text{With} \quad A = RGB_{Digital} \;\&\; B = RGB_{Film}$$

$$\text{And } M_{CC} = \begin{bmatrix} k_{11} & k_{12} & k_{13} \\ k_{21} & k_{22} & k_{23} \\ k_{31} & k_{32} & k_{33} \end{bmatrix} \text{ if considering a color correction with a 3x3 Matrix.}$$

To find the unknown M_{CC} matrix, we will use the Moore–Penrose[34] inverse defined as

$$M_{CC} = BA^{\top}(AA^{\top})^{-1} \qquad \textbf{Equation 3.2}$$

Yet, to improve the matching brought by the color correction matrix, we can base our correction on a 3x6 or 3x12 color correction matrix based on Root Polynomial Color Correction (RPCC)[35]. The dimension expansion introduced by this type of correction not only affects R,G,B but higher degrees of color combination such as $\sqrt{RG}\ \sqrt{GB}\ \sqrt{BR}$ for degree 2. Here is a list of the first 3 degrees of Root Polynomial expansions.

$$P_{1,3} = (R, G, B)$$
$$P_{2,3} = (R, G, B, \sqrt{RG}, \sqrt{GB}, \sqrt{BR})$$
$$P_{3,3} = (R, G, B, \sqrt{RG}, \sqrt{GB}, \sqrt{BR}, \sqrt[3]{R^2G}, \sqrt[3]{R^2B}, \sqrt[3]{G^2B}, \sqrt[3]{G^2R}, \sqrt[3]{B^2R}, \sqrt[3]{B^2G}, \sqrt[3]{RGB})$$

[34] R. C. Aster, B. Borchers, *Parameter Estimation and Inverse Problems*

[35] Finlayson, *Color Correction Using Root-Polynomial Regression*

This expansion gives more freedom for the color correction allowing non linearities in the datapoint matching.

While the higher degree RPCC improves results on points within the input data points, it doesn't show good results in points out of the input dataset. To cover those cases, we would need a dataset covering the entire gamut of our film and camera which is far to be the case with the Color Checker SG. Getting the locus of both of our systems will probably lower those issues and prevent overshooting in the correction of saturated colors.

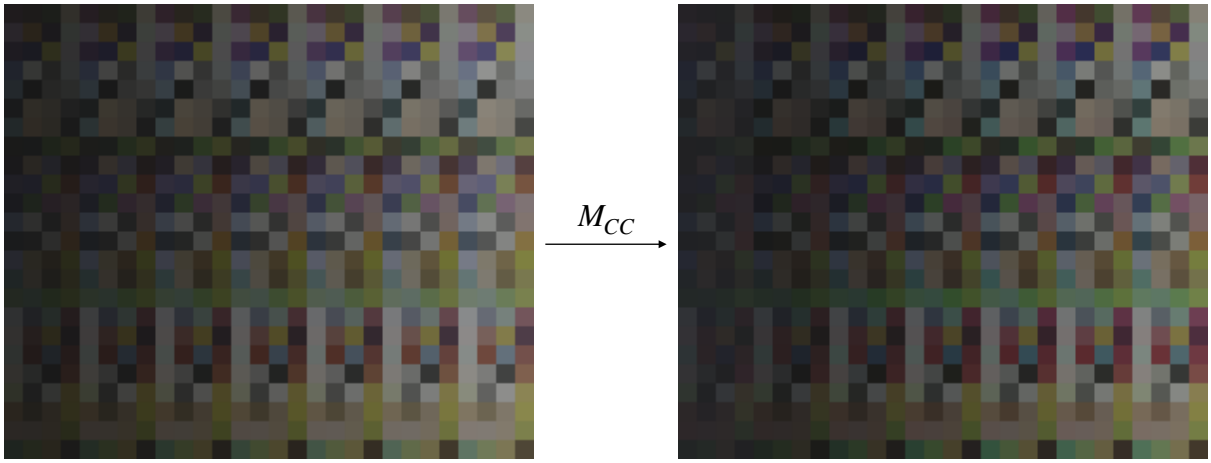

Figure 19 - Alexa 35 color DataSet to Film Color dataset transform

Giving the lack of highly saturated colors in our color dataset captured by our cameras and the relatively low number and diversity of patches, we get mitigated results and high deviations for saturated colors (out of the optimisation dataset). To limit errors in our Film Texture analysis, this matrix will replace the ACES AP0 To ADX10 only after texture synthesis when converting LogC4 to StatusM

NB: Indeed, reversing the ADXToLogC4 pipeline is manageable as all processing steps are matrices.We can do LogC4ToADX and even StatusM to apply Kodak2383 PFE (Print Film Emulation).

4 - Measuring film texture

4.1 Rendition of Detail

4.1.1 Slanted Edge method

4.1.1.1 Noise Dependency

The Slanted Edge method depends on the step function response of a given opto-electronic system. The principle of such a method is based on the Fourier decomposition of the signal thus giving its frequency component. The captured slanted edge is binned alongside a computed theoretical edge. The binned ESF is derived and Fourier transformed to get the frequency response of the captured signal (See Background). Binning alongside the edge allows us to lower the noise contained in the ESF thus allowing us to get a cleaner measure of the MTF. Yet, even with an average of around 4000 lines (the two sides of our slanted slit), noise remains important in the ESF. As a result, out-coming MTF are less precise and lower slightly the precision of our kernel retrieval optimization algorithm detailed in section 4.1.2.

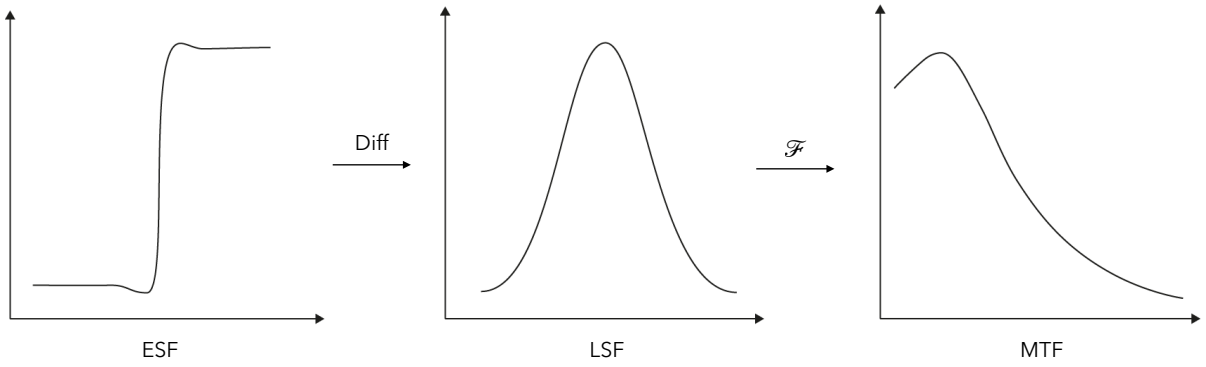

Figure 20 - Reminder Film MTF principle

Somewhat related to the noise/grain question, it has to be mentioned that the slanted edge method was primarily developed to avoid perfect alignment between the edge and the organized structure of a sensor. The 10° tilt avoids perfect matching with minor offset to a ground truth MTF[36]. Yet, if the method works great with a structured sensor, it has some minor downsides for stochastic acquisition devices such as film. As it can be seen in figure 21, the image of a sharp edge by a film emulsion has an inherent wiggle to it. To explain it, we can take a look at the silver halide structure that plays a role in the rendition of detail of a given film emulsion. Nevertheless, as fundamental particles (silver halides) have a size between 0.2 and 2 microns[37], the wiggle can only reach a value of 4 microns, independently from the measured «grain» size.

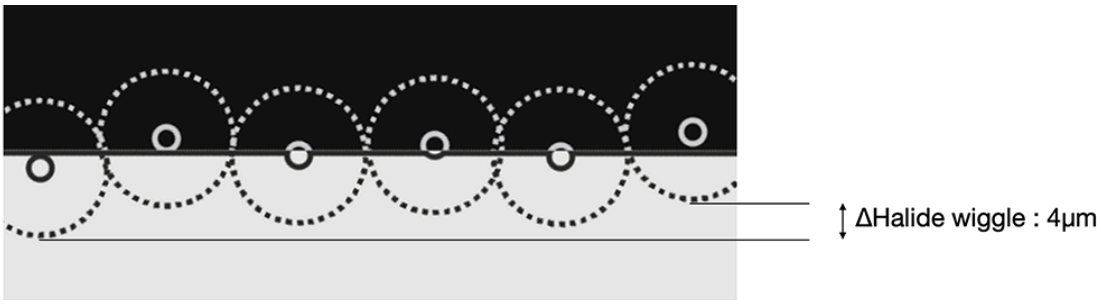

Figure 21 - Halide stochastic position or halide wiggle

This leads to a minor effect compared to other parameters affecting the rendition of detail such as Mie scattering and adjacency effect. The wiggle will then be considered irrelevant to correct as the impact should be rather small if non-existent.

4.1.1.2 Region of Interest

The size and content of the selected ROI around our hypothetical edge are quite important. To begin with, a too large region of interest might lead to inaccuracies if the MTF computation as residual noise artificially modifies certain frequencies of the spectrum. Yet, too small of a region and you're not getting an accurate

[36] Roland, Jackson K. M., *A Study of Slanted-Edge MTF Stability and Repeatability*

[37] Tim Vitale, *Film Grain, Resolution and Fundamental Film Particles, p.2*

representation of the MTF either, leaving adjacency effects and larger scattering effects unmeasured and lowering your resolution of your MTF by the same occasion. Given the expected size of blurring and sharpening effect you might get, you can tailor your region of interest size accordingly.

4.1.2 Optimisation

To retrieve kernels from MTF measurements, we opted for a least square optimisation based algorithm. As presented in the Background section, MTF is the Fourier Transform's magnitude of the derivation of the ESF. Being the magnitude, the MTF measurement prevents us of applying the inverse Fourier transform to retrieve a filtering kernel out of it. Furthermore, the MTF measurements being noisy even after binning, the least square optimization prevents having badly shaped and thus full of artifacts kernels.
As a reminder, the film rendition of details has been modeled as a concatenation of 2 physicochemical effects that are light scattering and adjacency effect (concentration gradient). It has not been clearly stated but scattering is considered to happen in linear domain and sharpening in logarithmic domain.
The processing considered pipeline is presented as such :

Figure 22 - Processing Pipeline RoD

With the Blurring and Sharpening kernels defined as such:

$Ker_{1D}(\sigma) = \frac{1}{\sigma\sqrt{2\pi}} e^{-\frac{1}{2}\left(\frac{x-\mu}{\sigma}\right)^2}$ defined as a Normal Distribution 1D Kernel

δ defined as a Dirac Kernel (or identity Kernel) and D detail level

$$Ker_{Blur}(\sigma) = Ker_{1D}(\sigma) * Ker_{1D}(\sigma)^{\top} \qquad \textbf{Equation 4.1}$$

$$Ker_{Sharp}(\sigma) = \delta + \left(\delta - Ker_{1D}(\sigma) * Ker_{1D}(\sigma)^{\top}\right) \times D \qquad \textbf{Equation 4.2}$$

As the 2 filtering Kernels are not operating in the same domain we will run our optimization by filtering a synthetic edge and computing its MTF. If the filtering was happening in one domain only, optimizing our kernels only based on their frequency response could have been a better solution. The optimization runs as such :

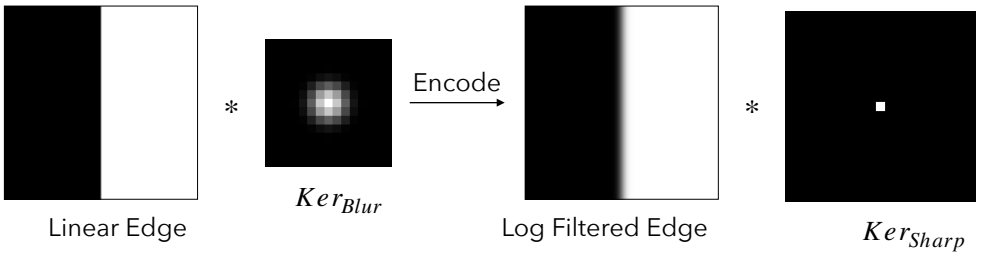

Figure 23 - Edge RoD processing for MTF computing for RoD optimization

According to a process that will be explained in section 5.2, Halation is added to our Synthetic edge that has been filtered twice (by Ker_{Blur} and Ker_{Sharp})

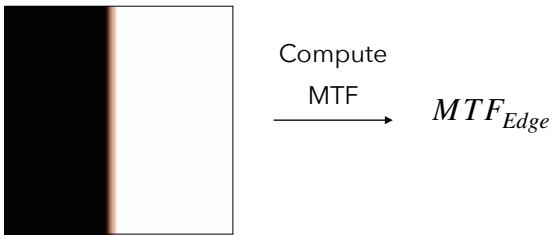

Figure 23 - Edge RoD processing for MTF computing for RoD optimization

Now that we have computed the MTF of our synthetic edge, we convolve it with the MTF of our digital camera which in our case has been considered to be the OLPF's MTF.

The cost function of the optimization algorithm is described as :

$$dist = \sqrt{\left(MTF_{Film} - \left(MTF_{Edge} \times MTF_{Alexa35}\right)\right)^2} \qquad \textbf{Equation 4.3}$$

$$\text{With } MTF_{Film} = \frac{MTF_{SlitFilm}}{MTF_{LensFilm}} \;\&\; MTF_{Alexa35} = \frac{MTF_{SlitA35}}{MTF_{LensA35}}$$

NB : In our case, $MTF_{SlitA35}$ was not ideally captured (lack of sharpness in the Blue channel) so we decided to use $MTF_{A35OLPF}$ instead.
Furthermore, both lenses' MTF, the one used on the Alexa35 and on the film camera, were measured with ARRI's MTF machine with the help of Dimitri Kloster from the optical department.

We run this optimisation on exposure ranging from 0EV to +5 EV (lower and higher exposures are either to noisy or not linear enough). The gives us 6 values for σ_{Blur} σ_{Sharp} and D. We average those 6 values to retrieve single parameters.

4.1.3 Preliminary Results

In this section we will present preliminary results of the optimization done to match the Alexa 35's rendition of detail to the film one (in this section 500T will be our target). As explained in section 4.1.2, we modeled film rendition of detail as a 2 step processing composed of 3 parameters per channel (BlurSize, SharpeningSize, DetailAmount). The algorithm was run on several exposures and here are some scatter plots resuming the outcome for each exposure level.

Color Negative Film

After minimizing, the MTF distances based on a least euclidean distance, we get kernel parameters for each exposure. Figure 24 presents the results computed to match Alexa 35 and Film.

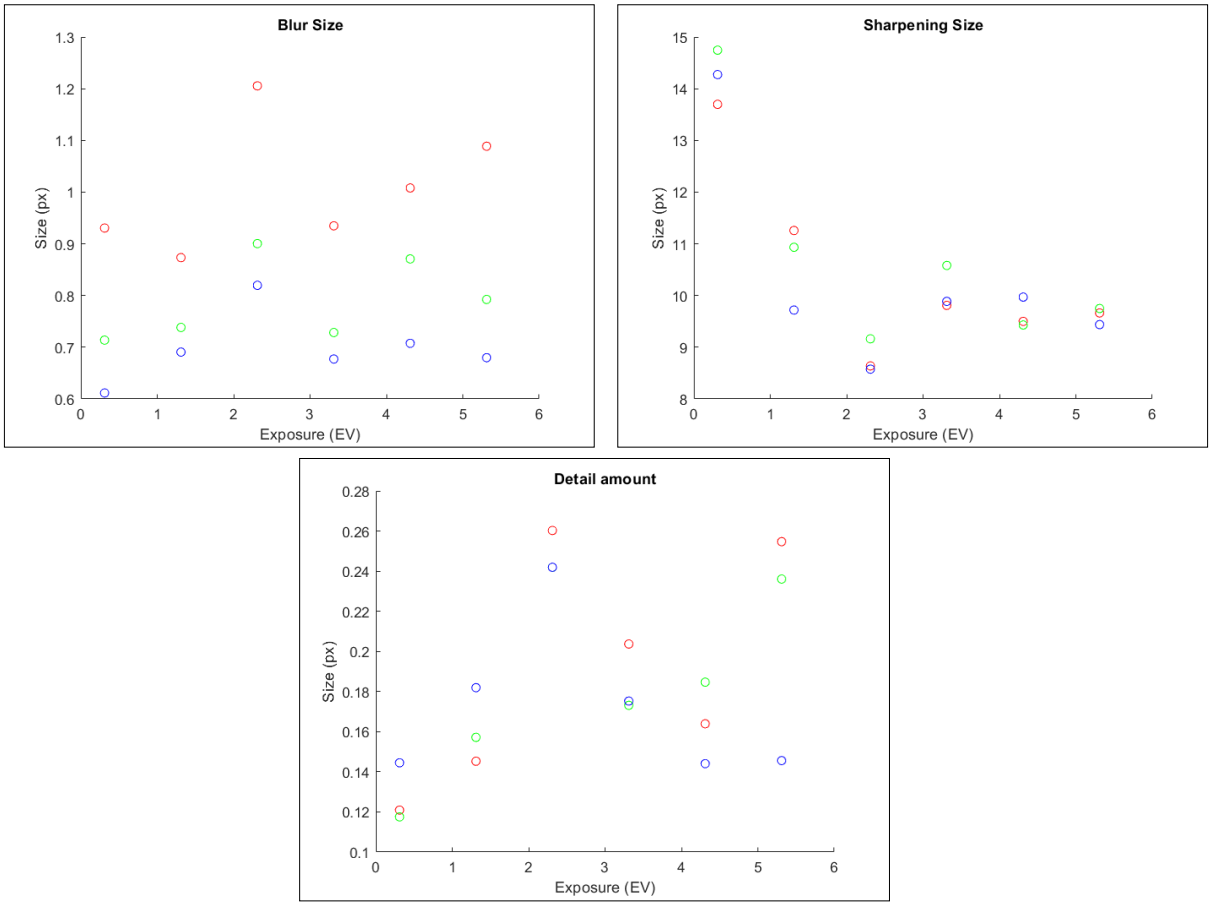

Figure 24 - RoD parameters from the optimization function - Input: Alexa35, Output: 500T

Even if the results clearly have a high standard deviation, we compute averages for each parameter and each color channel. We end up with a set of 9 parameters.

	R	G	B
σ_{Blur}	1	0,8	0,7
σ_{Sharp}	10,4	10,8	10,3
D	0,19	0,18	0,17

Figure 25 - Mean Parameters from RoD Optimization Input: Alexa35, Output: 500T

4.2 Halation

Halation was the most difficult film characteristic to get information about as there is not any documentation or scientific paper about it. Halation was considered an unwanted effect and was prevented thanks to antihalation layers located underneath the sensitive layers or at the very back of the film. As explained in the Background section, the film is partly responsible for these visual effects but is also responsible for the feasibility of registering optical characteristics brought by the optical lens itself.

4.2.1 Theoretical Hypothesis

As explained in the Background section, halation is multi-factorial and materializes numerous optical phenomena linked to the lens used as well as to the film itself. We will note here that the effects introduced by the lens are in no way visible in an image produced by a digital sensor and are made possible - just like the effects brought by the film itself - by the physical aspect of a film (in this case its thickness).

Presented below is the list of potential optical characteristics related to the shooting lens that may have an impact on halation. This section is not driven by citations or formulas as it is more an exercise of thought. No results from this section will be used in the upcoming synthesis.

The Aperture

In the image focal plane, the image points are considered to be points because they are smaller than the circle of confusion of the capture medium used. This point definition is only valid in a limited area defined as the depth of field. We then know that the point only exists if it is at a precise location, that is, a cone converges before the image focal plane and a cone diverges after it (for points in the focus plane and in front of it).

To simplify our model, we will only consider the sharp points of our image which then have a divergent cone after our emulsion. The aperture impacts not only the

quantity of light passing through the optic but also the depth of field by changing the image cone of a given point. The smaller the cone, the greater the depth of field. We can note that this impact of the aperture is visible in film thanks to its material nature since the thickness of the support then makes it possible to project this image cone onto the remjet layer.

To greatly simplify the complexity of multi-element lenses and because we are only trying to find evidences of the lens's impact on film, we are only considering a single-element lens. Thus, we are taking a simplified formula for the surface of the exiting rays from the back element of the lens.

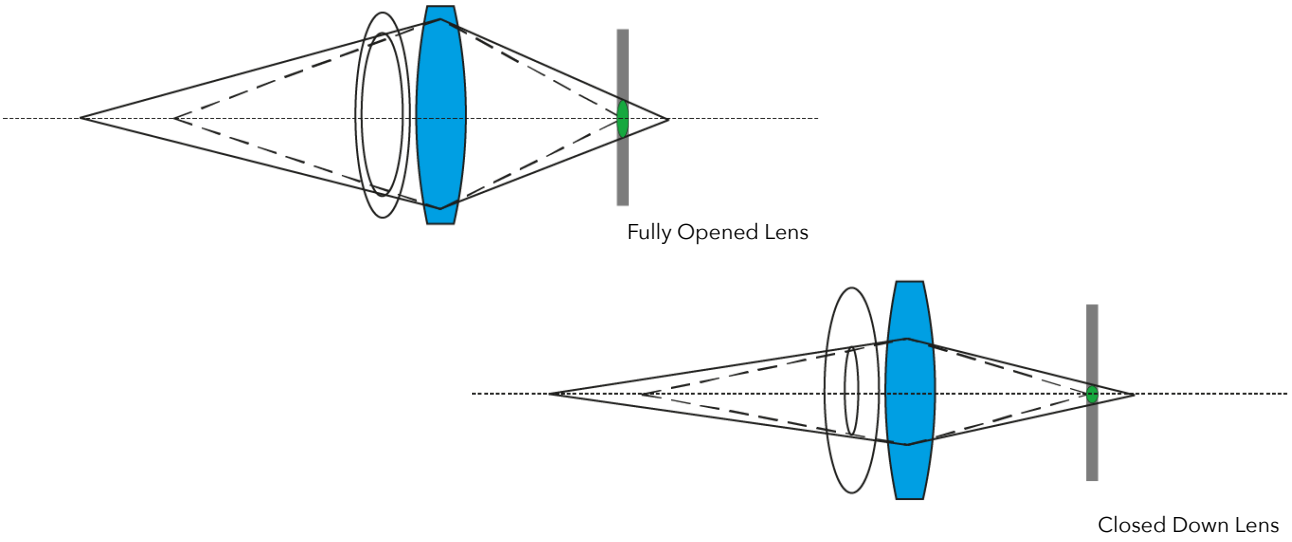

Figure 26 - Depth of field schematic

Vignetting

Vignetting does not seem, at first glance, to be a characteristic linked to the structure of the image, but only to its illumination. However, when we look into the reasons of vignetting, we notice that the reduction in illumination can be explained by the entrance and exit windows of our optics. The entrance pupils fulfill a role identical to the diaphragm of our lens: controlling the quantity of light passing through the optics as well as the depth of field around the considered point. We then deduce that, depending on the level of vignetting of our lens, the points located at the corners of our image will not have the same depth of field as those located in its center. We can even say that the stronger the vignetting, the greater the depth of

field in the corners of our image will be. Although not very visible on the image layer (if the sharpness is achieved carefully), we note that the projection of the image on the remjet layer is once again different depending on the position in the image. Points close to the optical axis are blurrier than points far from it.

NB: Note that it sounds counterintuitive to conclude that the corners of our image have a greater depth of field than its center and that consequently, the corners can be sharper. However, the performance declines regularly not due to the depth of field, but to the various aberrations present in an optic such as spherical aberrations, astigmatism, coma or field curvature.

Note also that for the vignetting modeling presented above, we consider the field curvature of the lens as non-existent and that the wavefront arriving on our film is perfectly parallel to it. We then consider vignetting to be only a phenomenon attributable to the entrance and exit windows.

Chief Ray Angle (CRA)

The principal rays of an optic are the rays passing through the center of the diaphragm. In practice, however, we consider the main ray to be THE ray passing through the center of the diaphragm and being at the limit of the coverage circle (considered as one of the angles of our image).

We note that the angle of the main rays with the optical axis increases linearly with the distance of the point considered from the optical center (for aplanatic spherical optics).

Although the CRAs are not without impact (problem of capture by the peripheral photosites receiving rays with too large an angle) on digital sensors and their problems are mainly addressed by the addition of micro-lenses, they materialize well. different on a silver photographic medium. The emulsion (sensitive surface) of the film is not impacted by the peripheral CRAs. However, due to the physical nature of the photographic film (its thickness), the image initially formed at the level of the emulsion and was then projected further onto the backbone of the film (at the level of the remjet layer). In the meantime, the rays have undergone other optical alterations which will be developed below. We then observe a phenomenon of centrifugal displacement: the points of the image being most impacted are proportional to their distance from the optical center.

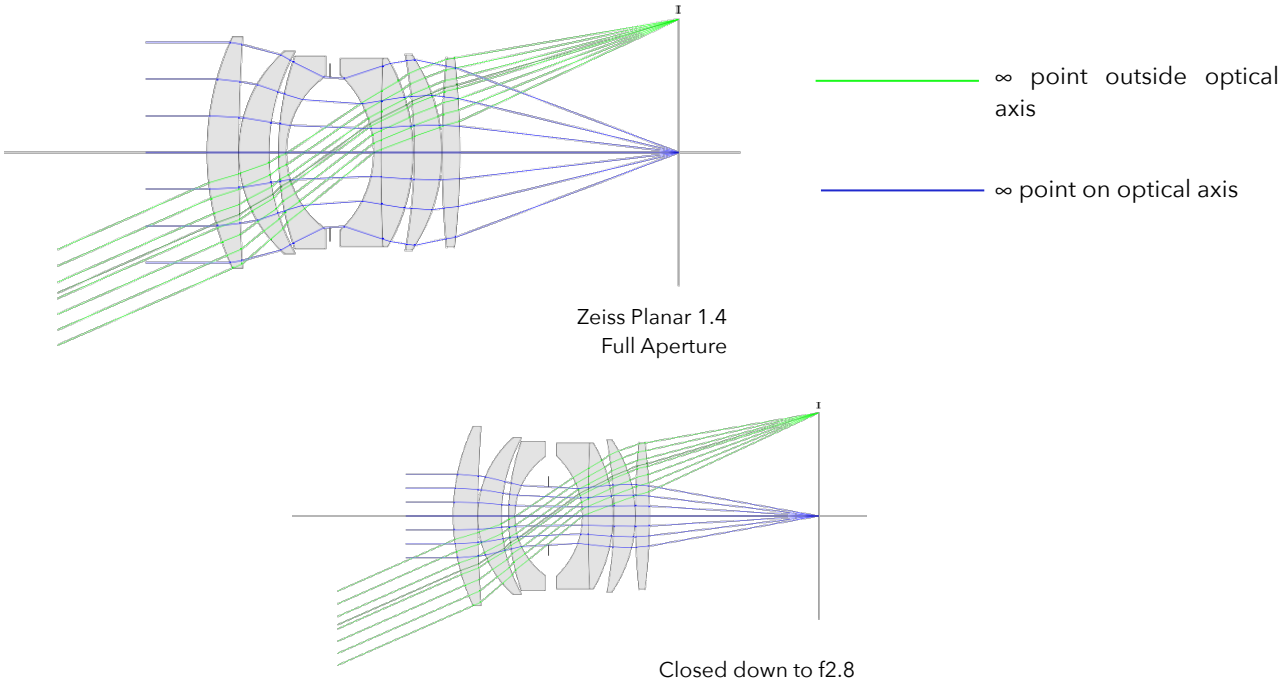

Figure 27 - Photons to Photos : CRA Schematic

Refraction

The refractive index of photographic gelatin and the film support itself has a refractive index of around 1.5. This optical property of photographic film then reduces a phenomenon mentioned previously. The angle of arrival of the rays coming from the rear element of our lens is then reduced. By applying Snell's laws, the image projected on the remjet layer is less distorted.

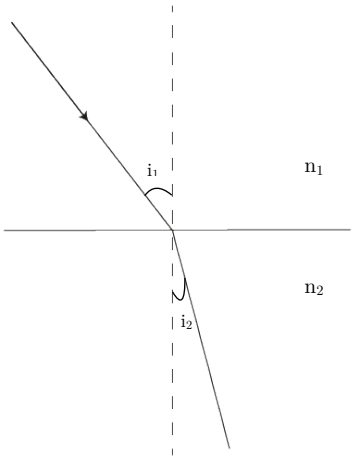

$$n_1 sin(i_1) = n_2 sin(i_2)$$

Figure 28 - Snell-Descartes's Law

Scattering and filtering

The multiple layers of gelatin loaded with silver halides coated on our film base strongly diffuse the light passing through our film. The sensitive layers of our film being composed of several million silver halide crystals, the light is scattered as it goes down into the support.

We consider, taking into account the size of the crystals considered (around one micron) and their optical characteristics, that their diffusion is close to Mie diffusion. However, given the complexity of modeling Mie diffusion and the uncertainty of the grain sizes, we decided to rely on actual measurement and not theory only.

This stage of modeling would require more extensive bibliographic research and scientific documentation and is not really the path we decided to explore for this master's thesis..

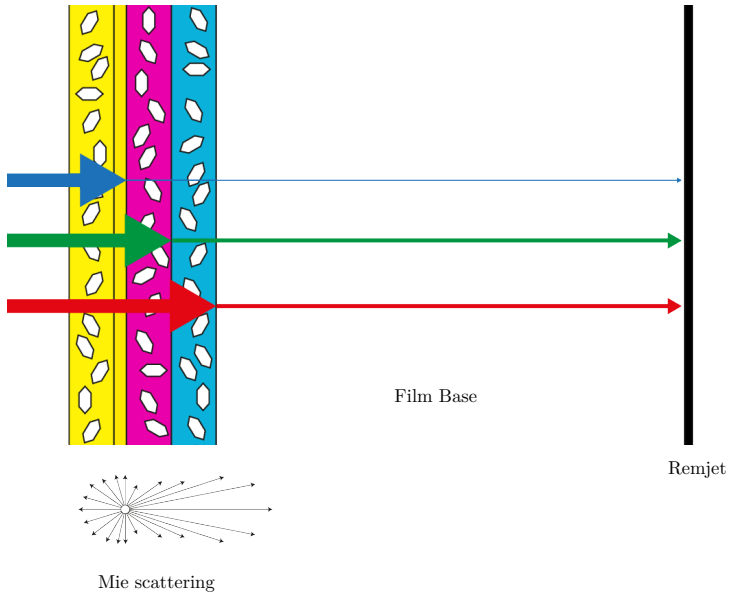

Figure 29 - Film Cut with layers and remjet, Mie Scattering.

To conclude, all those observations can be summarized in only one formula to compute the diameter of the unfocus disk at the center of the frame (not taking into account vignetting). This formula is not accurate due to simplifications by considering a single-element system instead of a multi-element lens. The exit

diameter is considered to be the same as the aperture blades (also being the same as the entrance pupil).

$$Angle_{Top/Bottom} = arcsin\left(\frac{sin\left(\pm\frac{1}{2}tan\left(\frac{1}{2\times A}\right)\right)}{i_{film}}\right) \qquad \textbf{Equation 4.4}$$

$$d_{Blur} = \pm 2B \times \arctan\left(Angle_{Top/Bottom}\right) \times r_{film}$$

Where B : Film base thickness (m), A : Lens Aperture (Numerical aperture), i_{film} : Film refraction index

4.2.2 Domain and Exposure Behavior

Due to the way we think halation is manifesting in film, we hypothesized early on that the effect should be additive in the linear domain. It seems, after all our experiments, that this is indeed correct.

We studied the region located 5 pixels away from the edge position (single point defined as the point where the gradient is the steepest positioned at N/2 being half the width of our ESF) to get the halation effect while avoiding the blurriness due the light scattering of the emulsion (being roughly 2 pixels wide). Yet, we were not out of the adjacency effect region being roughly 20 pixels wide. Unfortunately, choices had to be made and the spatial overlapping of these two effects was not avoidable.

We noticed that the ratio between the illuminated part of the slit and the selected pixel of interest was constant in the linear domain thus confirming the linearity of the effect in the linear domain.

$$\text{Considering } p = 5 \quad : \quad Hal_{Ratio}(E,c,p) = \frac{ESF\left(\frac{N}{2} - p, E, c\right)}{Slit(E,c)} \qquad \textbf{Equation 4.5}$$

with $E \in [-6,11]$ being Exposure and $c \in [R,G,B]$

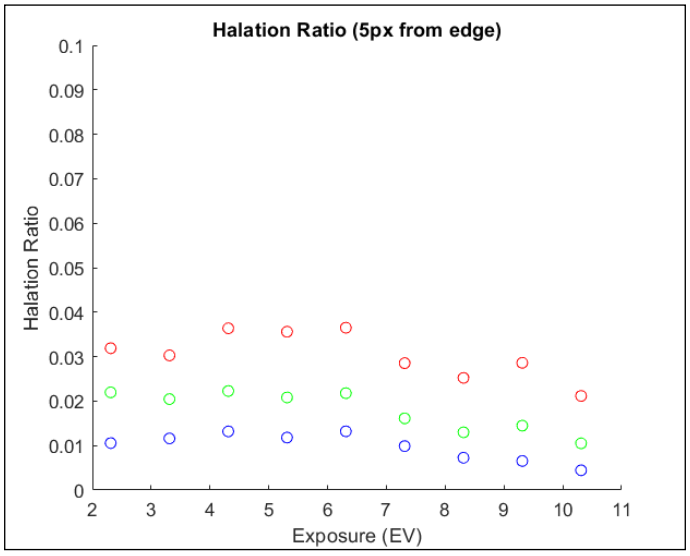

Figure 31 - Halation Ratio. (5px)

In the rest of section 4.2, we will consider the mean of Hal_{Ratio} on exposures +5 to +11 to be Hal_{Ratio} (as it is constant regarding to exposure)

$$Hal_{Ratio}(c,p) = \frac{\sum_{E=5}^{11} Hal_{Ratio}(E,c,p)}{7} \qquad \textbf{Equation 4.6}$$

4.2.3 MTF and Size

Properly measuring Halation Size was one of the most challenging questions we had to answer. We thought that halation would be measured in a meaningful manner in the MTF of higher exposures. Yet, we noticed that even if the MTF was indeed modified by halation, the concatenation of different phenomena made the number of parameters of our model too high and thus too unstable to optimize and was considered not reliable to retrieve both RoD and halation kernels out of it. Nevertheless, due to its quantifiable impact on MTF, Halation was taken into account in the optimization algorithm used to retrieve RoD parameters.

As explained in detail in section 4.2.1, prior geometrical simulations were done to get a global grasp of the effect. Yet, some wrong or at least inaccurate and not verifiable assumptions were made that have been retrieved from the section (see wrong assumptions in Figure 32 and next paragraph).

We thought that it was logical that the surface making contact between the remjet and the film base was indeed comparable to a Lambertian diffuser[38] thus obeying the cosin reflectance law. This however leads us to the conclusion that this highly diffusive surface was indeed still here after processing (remjet removing in ECN2) which was not the case. Indeed, film backing is quite smooth and the interface between the film and the remjet should be more specular than diffusive. Furthermore, it seems that the original approach of anti-halation was to neutralize unwanted light bounces by absorbing as much of the light as possible with dense black components not by highly diffusing it. Furthermore, spatial filtering light as a Lambertian diffuser would behave gave us results far from the effect we get from an actual film halation (see Appendix 3).

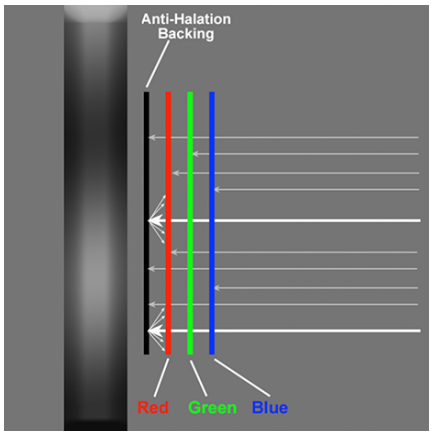

Figure 32 - Tobias Deml, Halation schematic

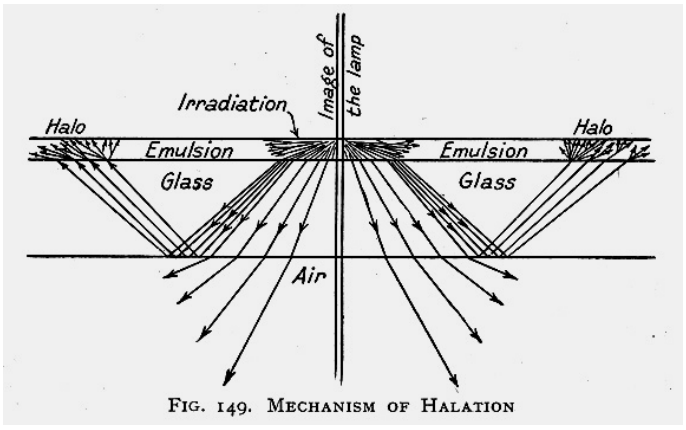

Figure 33 - L.P. Clerc, Photographic Theory – La Technique Photographique, Halation schematic

We did not take into account the impact of the hypothetical additional diffusion brought by the film's remjet/film-base interface and, as explained above, computed our halation size based on silver halide mie scattering in the upper layers.
We decided to rely upon prior RoD optimization results and more specifically the sigma of the blurring Kernels of the RGB layers. We extrapolated the scattering

[38] Janecek, Martin, et William W. Moses. *Optical Reflectance Measurements for Commonly Used Reflectors*

based on the film base thickness (standardized to 0.135mm for all film). Measurements of the film optical stack (layers) are provided in Appendix 4

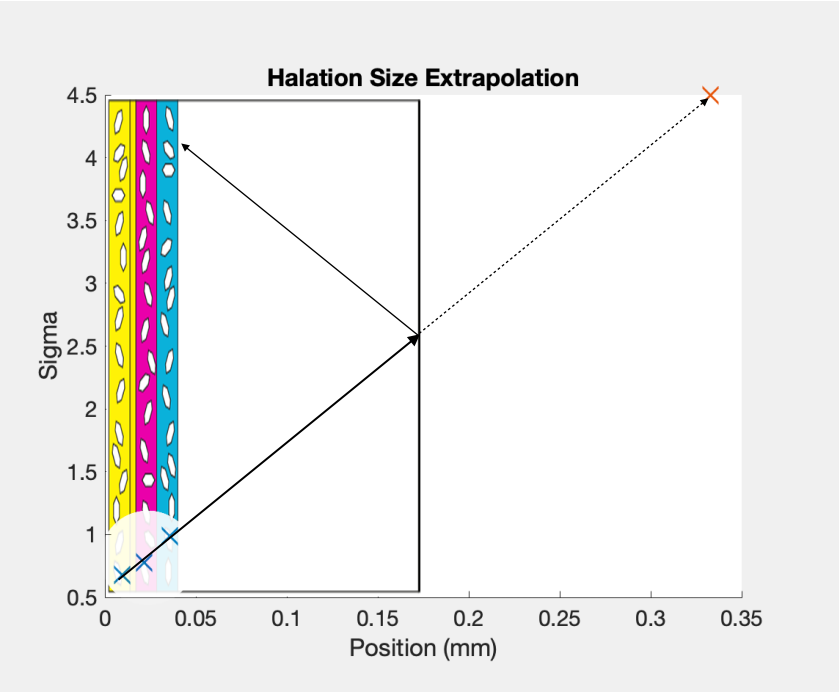

Figure 34 - Extrapolation Blur Kernels in Red, Blue and Green Sensitive Layers

This gives us an idea of the targeted Halation filtering kernel size yet the process is a bit unstable as the blurring measures are packed in a small region and we want to extrapolate a point far from those 3. Furthermore, it relies on the RoD optimization that itself relies on a Halation kernel size input to work properly. This conflict pushed us to consider another method based on the ESF.

As we explained in section 4.2.2, we consider the Halation process to be additive and increasing linearly in the linear domain. We thus decided to get samples of halation from 3 to 10 pixels away from our edge position. Their average ratios were computed by dividing them by their slit value (see Equation 4.6). We then took into consideration halation filtering impact based on a synthetic edge (Edge) of size N convolved with Gaussian kernels of increasing sigma (σ). Finding the right σ is

necessary to retrieve Halation Coefficient as the measured Hal_{Ratio} is not taking into account the Halation filtering kernel. The method is explained in Equation 4.7

$$\text{For } \sigma \in [4,8] : Hal_{Coeff}(c,p,\sigma) = \frac{Hal_{Ratio}(c,p)}{\left[Ker_{Halation}(\sigma) * Edge\right]\left(c, \frac{N}{2} - p\right)} \quad \textbf{Equation 4.7}$$

$$\text{with } p \in [3,10] \text{ being positioned from the edge (located at } \frac{N}{2})$$

From these Halation Coefficients, we compute standard deviations per filter sigma value (Equation 4.1). We're aiming for the lowest standard deviation as it assures us to get a linear behavior of the halation, no matter the position from the edge.

$$\text{For } \sigma \in [4,8] \ : \ \sigma_{Hal_{Coeff}}(c,\sigma) = \sqrt{\frac{1}{8} \times \sum_{p=3}^{10} \left[Hal_{Coeff}(c,p,\sigma) - \mu_{Hal_{Coeff}}(c,p)\right]^2}$$

Equation 4.8

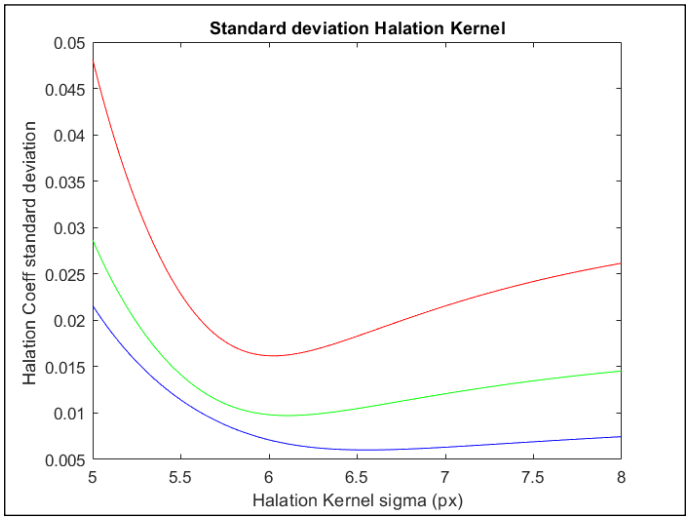

Figure 35 - Standard Deviation Halation Kernel
Halation Coefficient's standard deviation over Halation Kernel size

These results give us the standard deviation of the halation filtering kernel that allows equal halation ratios after correction. This method will be preferred over the extrapolation of the blurring kernel outputted by the RoD optimization algorithm.

$$\text{For } \sigma \text{ giving } Min\left[\sigma_{Hal_{Coeff}}(R,\sigma)\right]$$

$$Hal_{Coeff}(c,p,\sigma) = \frac{Hal_{Ratio}(c,p)}{\left[Ker_{Halation}(\sigma) * Edge\right]\left(c, \frac{N}{2} - p\right)} \qquad \textbf{Equation 4.9}$$

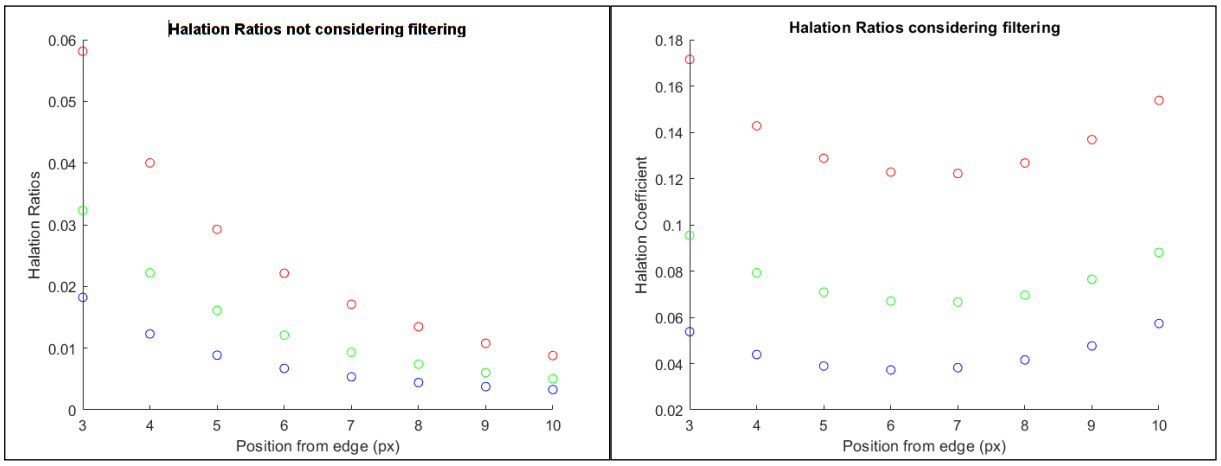

Figure 36 - Halation Ratios before and after filtering compensation

4.2.4 Color

As mentioned above, to measure properly the MTF response of our film, we decided to linearize it. Further than that, we even chose to operate a color space transform from film ADX10/APD to LogC4/AWG4 using the standard ACES pipeline with a customized linearizing LUT to better accommodate our own data set. Indeed, the domain in which the film spatial characteristics are synthesized is LogC4/AWG4 made for the Alexa35.

Halation being identifiable by its characteristic red/orange color, coming up with a way to characterize and reproduce it accurately was important.

As presented in the previous section, we optimized our kernel size to get the smallest standard deviation for the Halation Coefficients ranging from 3 to 10 pixels away from the edge (Section 4.2.3). Once we get the right kernel size, we can compute the Halation Coefficient as the mean of Halation Coefficients from position 3 to 10.

For σ giving $Min\left[\sigma_{Hal_{Coeff}}(R,\sigma)\right]$

$$Hal_{Coeff}(c,\sigma) = \frac{1}{8} \times \sum_{p=3}^{10} \frac{Hal_{Ratio}(c,p)}{\left[Ker_{Halation}(\sigma) * Edge\right]\left(c, \frac{N}{2} - p\right)} \qquad \textbf{Equation 4.10}$$

With $Hal_{Ratio}(c,p) = \frac{\sum_{E=5}^{11} Hal_{Ratio}(E,c,p)}{7}$ (see Equation 4.6)

Halation Coefficients are the result of normalized values Hal_{Ratio} and filtering corrected (section 4.2.3). They give us the level per channel of the Halation layer before it is filtered.

To conclude, halation is a linear increasing and additive effect in linear domain. Its size, while being extrapolable based on the RoD blurring kernel's size, is computed based on the film ESF points ranging from 3 to 10 pixels away for the edge and on a least standard deviation optimization. It has to be noted here that the first method was giving a halation kernel sigma with a 25% lower value than the second method. Color coefficients are computed from ratios corrected from the halation filtering impact.

4.3 - Grain

As previously mentioned, grain highly depends on the considered domain characteristics both in terms of color gamut and encoding curve. While space correlation remains pretty consistent across color space conversion, noise standard deviation, as well as channel correlation, are drastically modified. As a consequence, the extraction of film grain features to synthesize them on digital images has to be computed in the proper colorspace.
The digital camera mostly used for this thesis is the Alexa35, the colorspace chosen was LogC4/AWG4. Choosing this space mean that we can synthesize film grain straight on LogC4/AWG4 footage without any color space conversion and could be added after grading if it was done in the proper domain.

4.3.1 Noise Power

Noise Power is directly associated with noise sigma and might even be considered as a synonym. Film grain (B&W and Color negative film) can be described as a Gaussian noise which means it can be generated with a simple Normal Distribution with a given sigma and mu. Yet, this noise power is not constant throughout the exposure range. As with digital cameras, noise is directly linked to the signal level for various reasons. Furthermore, while both being analog, B&W and Color negative films do not have the same noise sigma to signal profile leading to different noise power.
Thanks to the protocol explained in section 2.2, and with a standard deviation computation detailed in equations 4.11, we're able to get the appropriate sigma LUT (Look Up Table with the signal as an input and noise standard deviation as an output).

$$\mu = \frac{1}{N}\sum_{i=1}^{N} x_i \qquad \sigma = \sqrt{\frac{1}{N}\sum_{i=1}^{N}(x_i - \mu)^2} \qquad Var = \sigma^2$$ **Equations 4.11**

4.3.2 Color correlation

Color correlation has been considered not relevant in the early stage of this thesis as we thought each film layer to be independent from one another. In addition, preliminary tests were done in black and white for cost and ease of development (rolls could be developed for the next day). Furthermore, the shadowing effect that might occur while scanning a color-negative film had been missed. Indeed, dye clouds from different layers could be on top of one another leading to strong layer correlation.

Pearson correlation coefficients[39] were used to characterize those interlayer dependencies. Pearson coefficients are formulated by Equation 4.12 and can be defined as the standard deviation weighted covariance of two datasets. In our case, the pairs considered are RG, GB and BR.

$$\rho_{X,Y} = \frac{Cov(X,Y)}{\sigma_X \sigma_Y} \qquad \textbf{Equation 4.12}$$

Pearson coefficients were useful when it came to measuring layer correlation but they did not allow us to find a straightforward formula that could decompose a correlated noise into a sum of three uncorrelated noise. Indeed, as explained before, we were crediting most of the correlation to be brought during scanning and coming from the stacked design of the film layers. With this hypothesis in mind, we thus chose to model our film grain as a sum of uncorrelated noise. The principle was simple and relied on generating three RGB uncorrelated White Gaussian Noises (that we will call driving noise) and correlating them later. The driving noise will be computed according to Equation 4.13

Equation 4.13

$$\begin{cases} Var(R_{input}) = Var(R_d + aG_d + cB_d) = Var(R_d) + a^2 Var(G_d) + b^2 Var(B_d) \\ Var(G_{input}) = Var(aR_d + G_d + cB_d) = a^2 Var(R_d) + Var(G_d) + c^2 Var(B_d) \\ Var(B_{input}) = Var(bR_d + dG_d + B_d) = b^2 Var(R_d) + c^2 Var(G_d) + Var(B_d) \end{cases}$$

[39] Pearson Coefficient defines the linear correlation between 2 dataset : Definition

With $Var(RGB_{input})$ the variance of the measured Film Noise per channel (correlated), and $Var(RGB_d)$ the variance of the driving noise (uncorrelated).

a, b and c coefficients will be obtained through an optimisation algorithm to minimize the Euclidean distance (Equation 4.14) between input and output Pearson Coefficients. The variances of the driving noised will be obtained by resolving the system such as presented in appendix 5.

$$d = \sqrt{(\rho_{R,G\ Input} - \rho_{R,G\ Output})^2 + (\rho_{G,B\ Input} - \rho_{G,B\ Output})^2 + (\rho_{B,R\ Input} - \rho_{B,R\ Output})^2}$$

Equation 4.14

$Input$ being the targeted Noise and $Output$ the noise at the current iteration of the optimization

4.3.3 Auto Correlation and Noise Power Spectra

Film grain can not be described only by its power and layer correlation. Spatial correlation plays a big role in what makes generated film grain look right. Spatial correlation is directly related to grain size but also takes into account the concatenation of the Opto-Electonic device used. A single grain is considered as a small homogeneous region leading to a point highly correlated with its neighbors. To measure this characteristic, we need a large homogeneously lit texture-free surface to compute the spatial correlation between a given pixel and its neighbors.
Current literature gives different and theoretically similar methods to analyze spatial correlation.
Auto Correlation is based on the covariance between a given point and its neighbors in a given neighborhood (detailed in Equation 4.15). This gives you a 2D map of the neighborhood with higher figures when the correlation is high.

Let's consider a grain plate (or noisy flat flied) I of size N. In order to compute the Auto Correlation of that grain plate, we need to consider E defined as the our grain plate which has been mean subtracted.

$$E(c) = I(c) - \mu_I(c) \quad \text{With } c \in [R, G, B]$$

For the computation of μ_I, see Equations 4.11

The Auto Correlation of this average subtracted grain plate is defined in Equation 4.15

$$\mathcal{A}(x, y, c) = \frac{1}{N^2} \sum_{a=1}^{N} \sum_{b=1}^{N} E(a, b, c) \times E(a + x, b + y, c) \qquad \textbf{Equation 4.15}$$

Where $[x, y] \in [-7, +7]$, $N = SizeSampledRegion$, $c \in [R, G, B]$

...

	a-2,b-2	a-2,b-1	a-2,b	a-2,b+1	a-2,b+2	
	a-1,b-2	a-1,b-1	a-1,b	a-1,b+1	a-1,b+2	
⋮	a-2,b-2	a-1,b-1	a,b	a,b+1	a,b+2	⋮
	a+1,b-2	a+1,b-1	a+1,b	a+1,b+1	a+1,b+2	
	a+2,b-2	a+2,b-1	a+2,b	a+2,b+1	a+2,b+2	

...

With a,b being the position of the considered pixel.

Figure 37 - AutoCorrelation Neighborhood

Likewise, to get the spatial correlation between layers, Cross Correlation is defined as

$$\mathcal{C}(x, y, c_1, c_2) = \frac{1}{N^2} \sum_{a=1}^{N} \sum_{b=1}^{N} E(a, b, c_1) \times E(a + x, b + y, c_2) \qquad \textbf{Equation 4.16}$$

$$\text{Where } [x, y] \in [-7, +7],\ N = SizeSampledRegion,$$
$$c_1 \in [R, G, B],\ c_2 \in [R, G, B]\ \&\ c_1 \neq c_2$$

The AutoCorrelation was investigated at a later stage in the analysis of noise spatial correlation and NPS was the main mathematical tool used to measure this noise characteristic. Yet, the results were not there as we were not having enough sample points in our original measuring method. The method consisted in taking the Fourier Transform of the entire grain plate and averaging spatially in the Fourier domain to reduce noise impact on the measurement. Several methods using subsampling in spatial domain and overlapping samples were also tested to investigate and find the method most suited to our measurement but without any noticeable improvement.

$$NPS = \frac{1}{N^2} |\mathcal{F}(E)|^2 \qquad \textbf{Equation 4.17}$$

Furthermore, the NPS being the magnitude of the Fourier Transform, we lose information in the process and are unable to apply an Inverse Fourier Transform to retrieve a filtering kernel. Our early method[40] was based on an optimization in frequency domain between the $\sqrt{NPS}$ and the frequency response of a filtering kernel (being a mix of blurring and sharpening kernel). The results obtained were fine, but the optimization process was tedious for no good reason. Last but not least, the Wiener–Khinchin theorem gives the direct relationship between AutoCorrelation and NPS as shown in equation 4.18 which gives hope of finding a proper method to extract filtering kernels straight out of our grain plates.

$$\mathcal{A} = \mathcal{F}^{-1}(NPS) \qquad NPS = \mathcal{F}(\mathcal{A}) \qquad \textbf{Equations 4.18}$$

The formula used for the kernel computation in a normal AutoCorrelation method on a mean subtracted grain plate. To get a usable filtering kernel and get rid of remaining offsets in the AutoCorrelation matrix, the furthest neighbors from the characterized point are averaged and subtracted from the AutoCorrelation

[40] S. Eckel, P. Huthwaite, U. Zscherpel, A. Schumm and N. Paul, *Realistic Film Noise Generation Based on Experimental Noise Spectra*

measurement. To get the expected frequency response, the AutoCorrelation matrix is squared to get the right filtering Kernel. For an AutoCorrelation matrix of size N we get :

$$Ker_c = \left[\mathscr{A}(c) - \frac{\left[\mathscr{A}(1,1,c) + \mathscr{A}(1,N,c) + \mathscr{A}(N,1,c) + \mathscr{A}(N,N,c) \right]}{4} \right]^2 \text{ with } c \in [R,G,B]$$

Equation 4.19

Similarly

$$Ker_{c_1c_2} = \left[\mathscr{C}(c_1,c_2) - \frac{\left[\mathscr{C}(1,1,c_1,c_2) + \mathscr{C}(1,N,c_1,c_2) + \mathscr{C}(N,1,c_1,c_2) + \mathscr{C}(N,N,c_1,c_2) \right]}{4} \right]^2$$

$$\text{with } c_1 \in [R,G,B] \text{ , } c_2 \in [R,G,B] \text{ \& } c_1 \neq c_2$$

Equation 4.20

4.3.4 Preliminary Results

In this section, we will present some results that have been obtained by running an algorithm managing the color space transform as well as extracting the grain characteristics of our scanned film and digital footage. This section will cover only the results of 500T for the film and the Alexa 35 shot with an EI of 200.

Color Negative Film

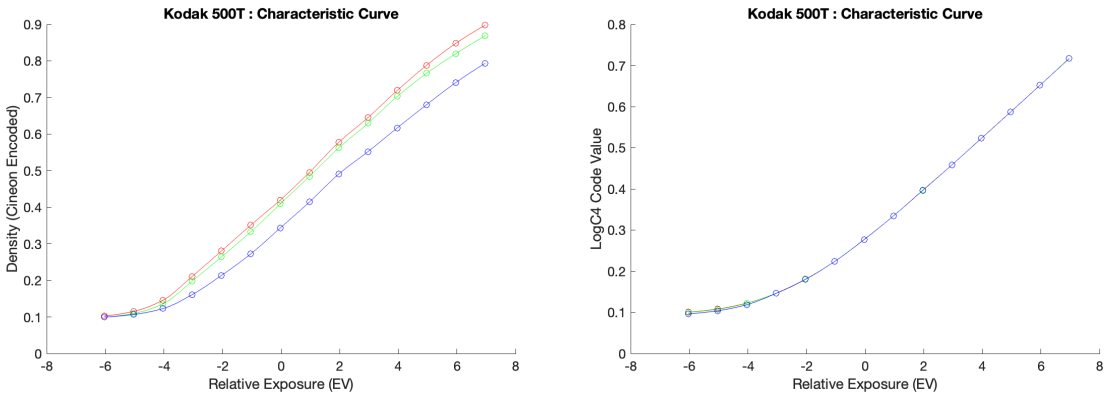

38 - 500T Characteristic Curve linearized

As previously introduced, the process of film linearization is white balancing the signal while linearizing it. The results of the linearization are shown in LogC4. Furthermore, we decided to only plot the part before the shoulder as the noise was skyrocketing due to the heavy gain necessary for those last stops to maintain a linear behavior.

The higher gain factors necessary to linearize the shoulder of the film characteristic curve are directly visible in the sigma noise plots presented in Figure 39 and more specifically the shape modification.

Interestingly, we get an opposite trend with midrange values that are indeed reduced by the linearization yielding lower Sigma Noise in LogC4 than in Cineon.

Overall, we observe a higher slope in density domain thus leading to a global sigma reduction in LogC4 domain after linearization.

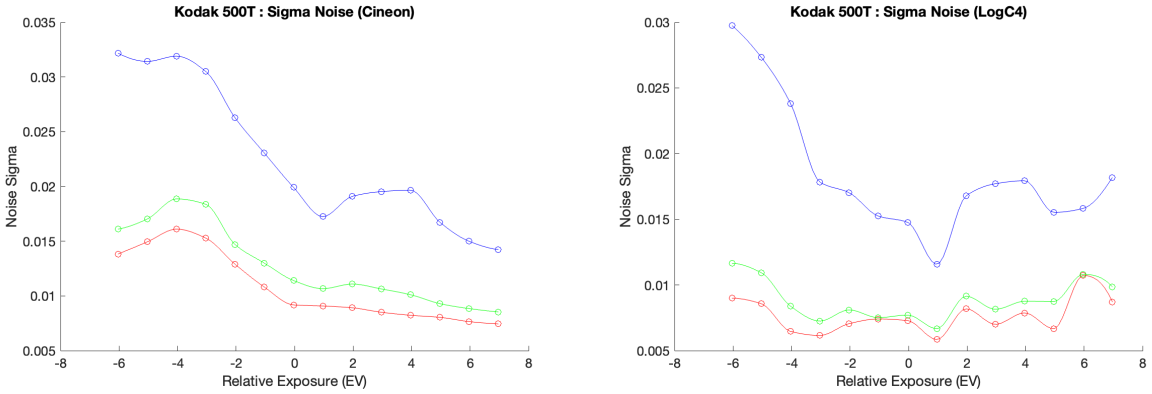

Figure 39 - Noise sigma (power) before and after linearization and LogC4 encoding

Noise has a relatively stable power throughout the exposure range with its max and min values being a factor 2 from one another.

Spatial-wise, the film presents spatially correlated noise with filtering kernels derived from the computed AutoCorrelation (R,G,B) and CrossCorrelation (RG,GB,BR) displayed in Figure 40

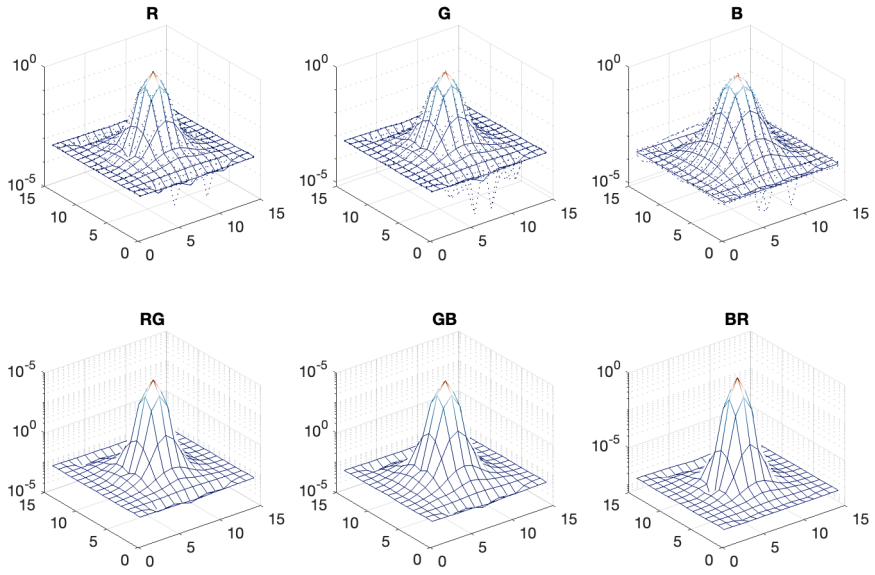

Figure 40 - 500T Grain Spatial Correlation - Log scale

NB : The Autocorrelation kernels are ploted in log domain to see precisely the low values of the kernel. Yet, It might over-emphasize them giving a wrong visual representation of the Kernel.

In the FrequencyResponse plots (Figure 41) computed from the AutoCorrelation Kernels, we can notice bigger grains in the blue-sensitive layer, red and green being smaller and rather similar.

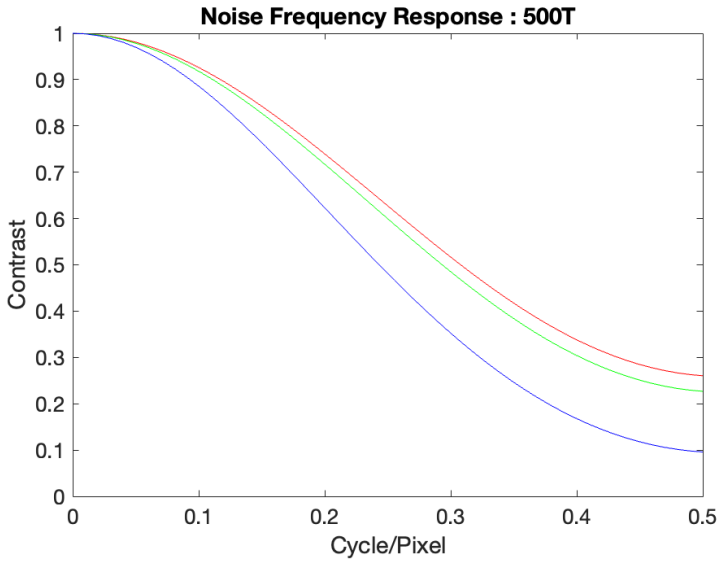

Figure 41 - Noise Frequency response averaged (and 1D)

One of our results slightly surprised us as we introduced a diverging hypothesis in the Background section with grain size (halide crystal) and spatial correlation for color negative film. As a reminder, the hypothesis that grain size (developed dye cloud)was unrelated to the halide it originated from. However, according to Figure 42 we can see a tendency of decreasing grain size when exposure increases.

Figure 42 - Noise spatial Correlation size 500T

NB : Noise Loss is a metric that has not been introduced yet. It has not been explained in the Background section because it's more of a homemade metric that we find relevant and useful.
The metric can be defined as such :

Let's consider $Noise_{input} * Ker = Noise_{Output}$
with $Noise_{input}$ being any Noise

$$NoiseLoss = \frac{\sigma_{Input}}{\sigma_{Output}}$$

With σ_{Input} being the standard deviation of $Noise_{input}$ and σ_{Output} of $Noise_{Output}$

NB: The layer correlation coefficients obtained with equation 4.14 are not shown because they are constant over the entire exposure range.

Alexa 35

Running the algorithm on the flat field ramp images we captured with the Alexa35 at EI200 this time and we found drastically different results in terms of noise reparation this time. We can see low noise in the lower and upper end of the exposure range with the highest values being located in the shadow section (ranging from -6 to 0 stops). The small regain of noise amount at +2 stops *might* be a consequence of the dual gain sensor that is the Alev4.

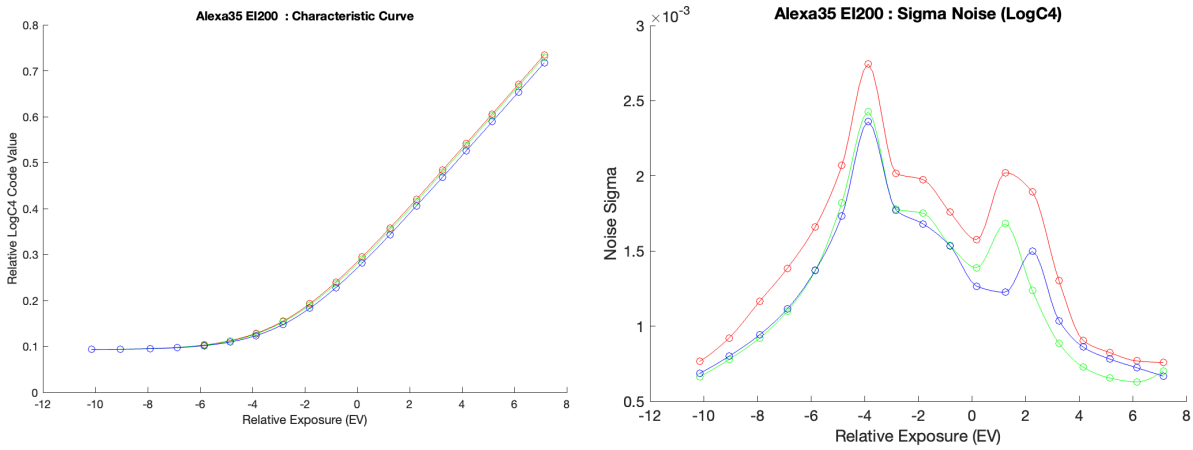

Figure 43 - Characteristic curve and noise Sigma, Alexa 35 EI200

The mean noise spatial correlation is as expected from a debayered sensor with higher spatial correlation for the Red and Blue. Indeed, their resolutions (pattern in the Bayer CFA) are half the one of the Green channel thus increasing the size of the spatial correlation. Green logically gets a lower spatial correlation as it has a higher resolution. Furthermore, images are additionally filtered by the standard Alexa 35 texture modifying the spatial correlation of each channel.

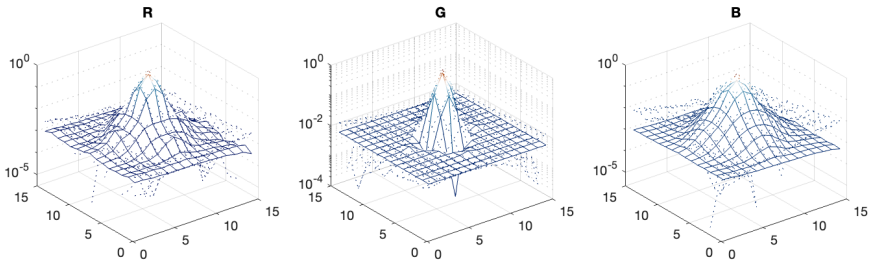

Figure 44 - RGB noise spatial correlation Alexa 35 EI 200

In the following noise spatial correlation plots, we can not identify a correlation between grain size and exposure. We can yet identify a noise loss decrease at +1 EV in the Red channel being created by a sharpening behaviors identified at that exposure level. Overall, Blue layers present similar grain size between

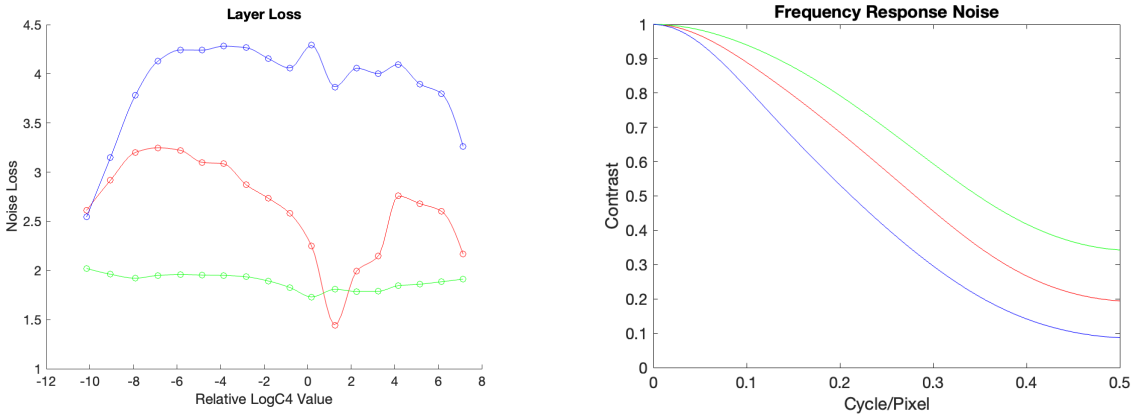

Figure 45 - Alexa 35 EI - 200Spatial Correlation per exposure and average Frequency Response

Layer correlation results coming from our optimization algorithm based on Pearson Coefficients and the theoretical model behind it does not work for this type of noise. As Bayered raw data shows uncorrelated noise spatial-wise and channel-wise (RGB channels don't even exist yet), debayering correlates noise in both ways. This means that are sum of uncorrelated noise to model film grain doesn't hold up anymore as a more advanced process takes place in the noise correlation of the Alexa 35. The algorithm struggles to find a plausible outcome for the optimization thus giving erroneous results (not dispalyed here).

5 - Emulation of film texture

5.1 Rendition of Detail

As a reminder, we built Rendition of Detail based on classical filtering techniques both in linear and logarithmic domains. As explained in section 4.1, we based our analysis on MTF curve fitting by minimizing the Euclidian distance of a target and an input MTF. In our case, our target MTF was film while the input one was Alexa35. The model our optimization was based on was a mix of filtering in linear domain for blurring and logarithmic domain for sharpening while taking into account halation.

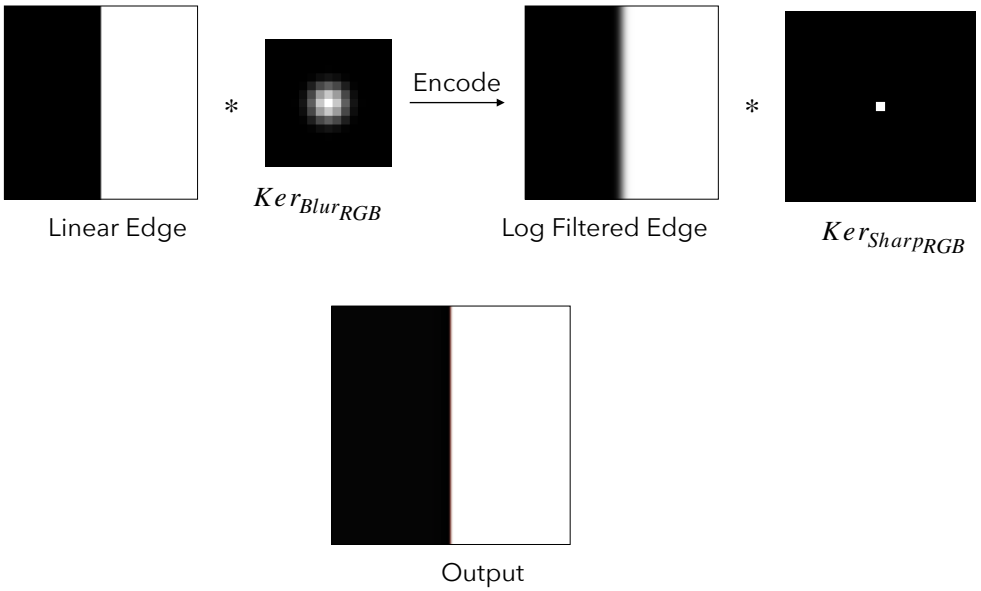

Figure 23 - Edge RoD processing for MTF computing for RoD optimization

Kernels are generated based on Equations 4.1 and 4.2

5.2 Halation

The halation processing pipeline has not been fully described yet and many characteristics have been introduced in section 4.2 but no processing model has been given. We can describe the pipeline as :

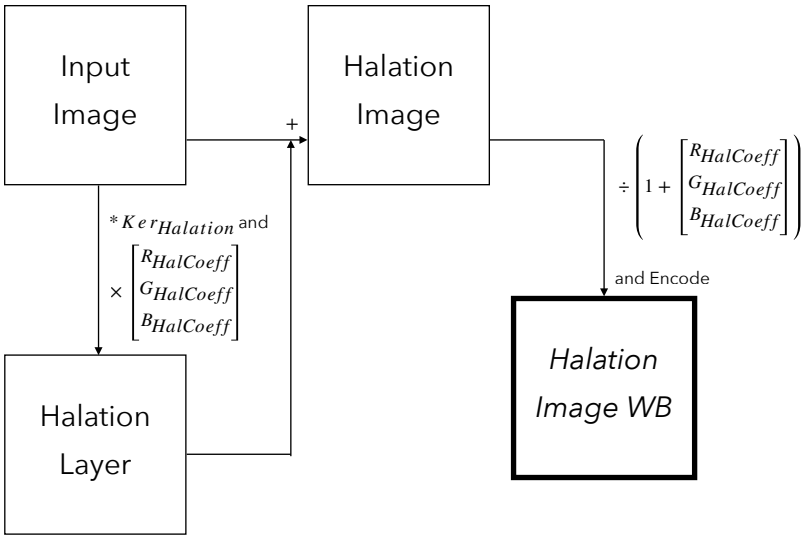

Figure 46 - Halation processing principle

The Halation processing is straightforward and relies only on a single-size kernel filtering as well as the Halation coefficients previously computed.

NB: The division by the Halation coefficients at the later step assures grayscale values consistency after processing. This is recommended as if not considered, the exposure as well and the grayscale value will vary drastically.

5.3 Grain

After running our analysis algorithm on our film footage and retrieving results presented in section 4.3.4, we can start and think about an algorithm that will allow us to synthesize the grain structure we just analyzed.

The measures we retrieve are discrete and need to be interpolated and extrapolated to cover the full LogC4 range [0,1].
Different methods are applied depending on the noise characteristic we want to extrapolate.

Sigma LUT

The sigma LUT describes the relationship between the input LogC4 code value and the standard deviations or the driving noises (in RGB) associated with it. The lower end is extrapolated based on the noise sigma of the base+fog, the upper end is extrapolated with a target standard deviation noise of 0 as the max LogC4 value being considered noise-free.
LogC4 maximum value is located at +11.35 stops above gray point and Film maximum value has been considered to be located around +7 or 8 stops as the nonlinearity of film becomes too important.

Layer Correlation

Layer correlation coefficients are constant throughout the exposure range. We will then use an average value for each channel correlation between RG, GB and RB.

Spatial Correlation - Grain Size

As shown in Figure 42 grain size varies with exposure. If a noise sigma LUT is easy to implement in a program, varying filter sizes depending on code value is more challenging as the computational time is largely multiplied. To mitigate this computational issue, we decided to create a second processing pipeline relying on a single averaged kernel for each channel. We then end up with single-size grains as a compromise of computation time.

5.3.1 Noise generation

At the beginning of the process, AWGN is reduced and centered ($\mu = 0$ and $\sigma = 1$) is generated. At that stage, the grain is completely uncorrelated. We multiply our noise

with our image that has been run through the Noise LUT (Input being LogC4 values, and output being sigma noise values). We can remind here that :

$$\mathcal{N}(\mu,\sigma) = \mathcal{N}(0,1) \times \sigma + \mu \qquad \textbf{Equation 5.1}$$

We end up with an AWGN that has a standard deviation related to the LogC4 code value of the pixel it is associated with in every point of the image.

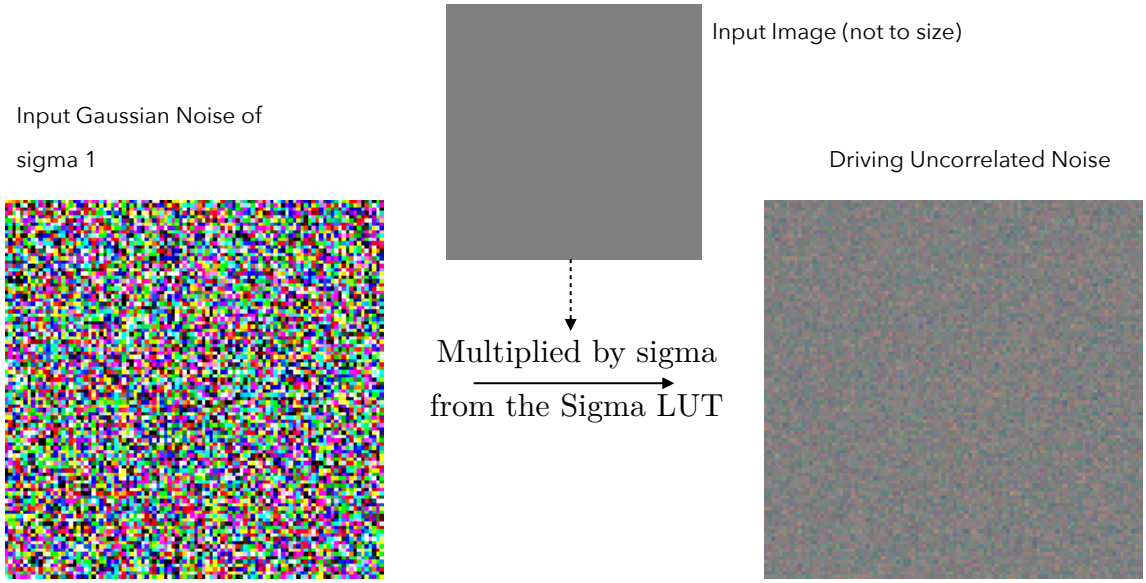

Figure 47 - Noise Generation Noise Sigma LUT processing

Here is an Equation to resume our former explanations

$$[R_d, G_d, B_d] = \mathcal{N}(0,1) \times LUT_{Noise\sigma}\left(Image_{Input}\right) \qquad \textbf{Equation 5.2}$$

with R_d, G_d, B_d being the driving noises for each channel

5.3.2 Filtering

Filtering AWGN allows it to be spatially correlated giving it more grain visual attribute. In our algorithm, the filtering step is happening jointly with the Layer correlation. As introduced in section 4.3.2, each layer is considered to be an addition of several layers (see Equations 4.19 and 4.20 for Kernel definitions).

$$\begin{cases} R_{Noise} = R_d * Ker_R + aG_d * Ker_{RG} + bB_d * Ker_{RB} \\ G_{Noise} = aR_d * Ker_{RG} + G_c * Ker_G + dB_d * Ker_GB \\ B_{Noise} = bR_d * Ker_{RB} + cG_d * Ker_{GB} + B_d * Ker_B \end{cases}$$ **Equation 5.3**

with a, b, c being layers correlation coefficient (respectively RG, GB, BR)

Ker_R, Ker_G, Ker_B being the filtering kernels respectively for R,G,B driving Noises

$Ker_{RG}, Ker_{GB}, Ker_{BG}$ being the filtering kernels respectively for R,G,B driving Noises

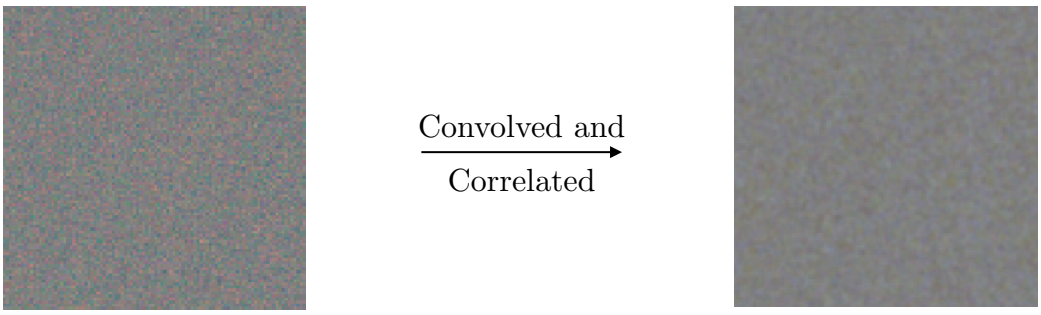

Driving Uncorrelated Noise

Filtered and correlated Noise/Grain

Figure 48 - Noise Filtering and Correlation

5.4 Overview

As explained in the previous sections, the film texture emulation works with 3 separate processing steps which are directly linked to the RoD, Halation and Grain. These characteristics must be added to the digital footage in this specific order to guarantee the correct film texture look.

See Appendix 6 for a full and more detailed schematic of the entire pipeline.

As in previous sections, let's take a perfect edge (-4 & +4 EV for dark and bright side and filtered to match original Alexa 35 MTF) and process it through the entire pipeline :

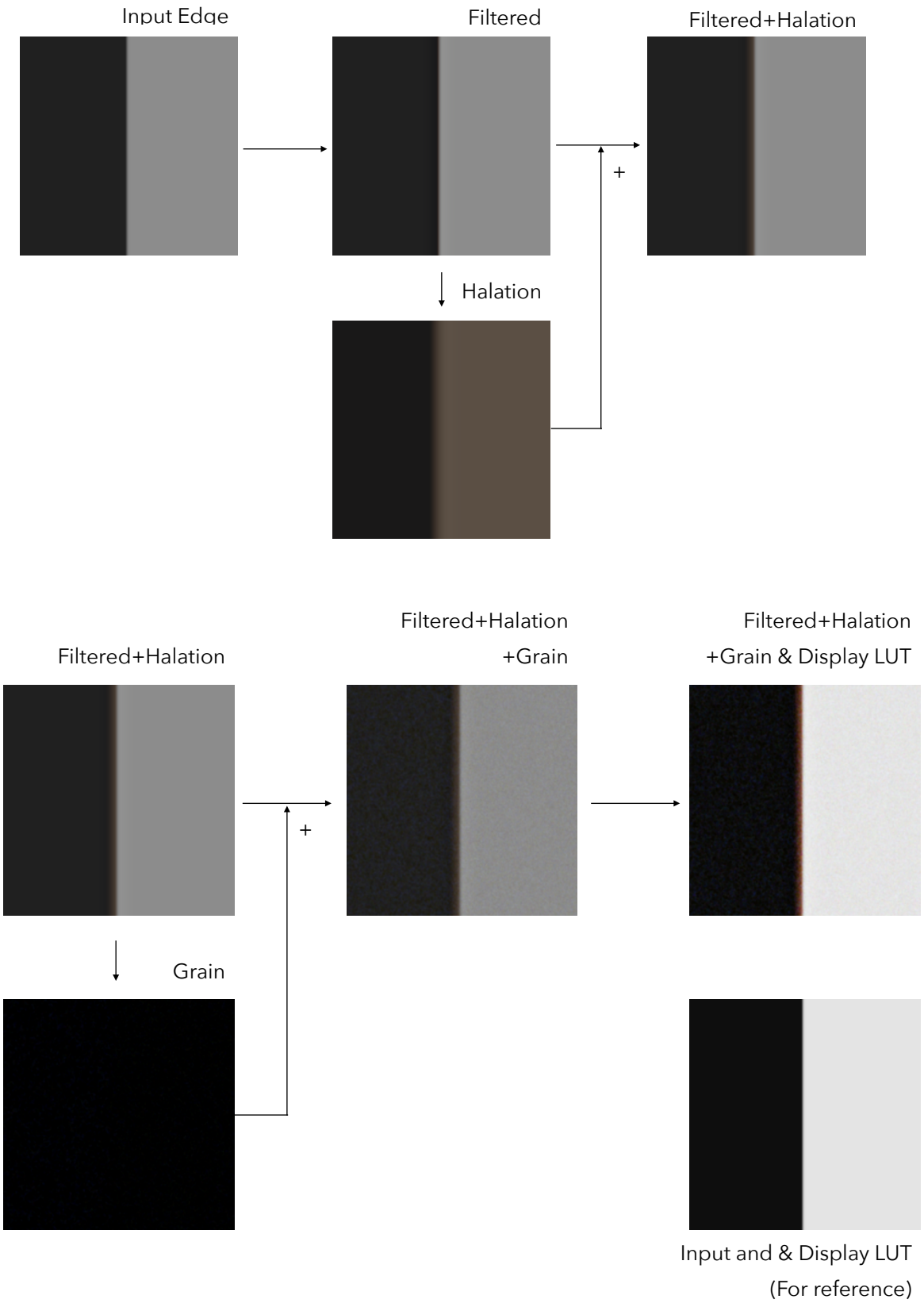

Figure 49 - Entire processing pipeline on a synthetic edge

6 - Evaluation

We have already seen that early results from the synthesis section are promising. This section is meant to present objective results through measures and plots but also visually. Yet, it has to be stated that this part could be a thesis on its own. Indeed, as we have approved metrics to measure color differences, RoD and Halation do not benefit from these specific and psycho-perceptive metrics. Furthermore, assessing data with people and not measures requires building rigorous evaluation protocols and evaluation datasets. We have built an assessment dataset that would benefit from motion (we only shot stills) and more importantly, diversity of scenes. This would involve shooting with a rather big crew and creating elaborate scenes to get the most out of the assessment.

6.1 Objective measurements

6.1.1 Noise Analysis

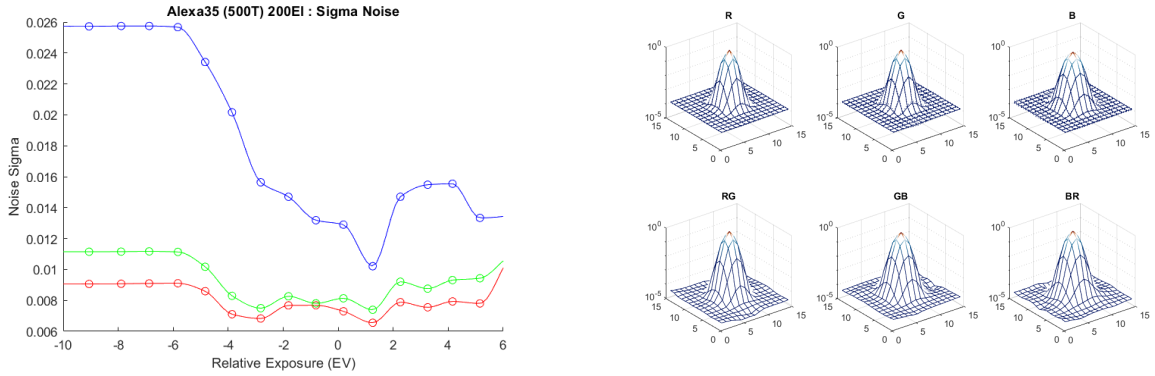

Figure 50 - Sigma Noise and Spatial Correlation of emulated film texture on Alexa 35 @ EI 200

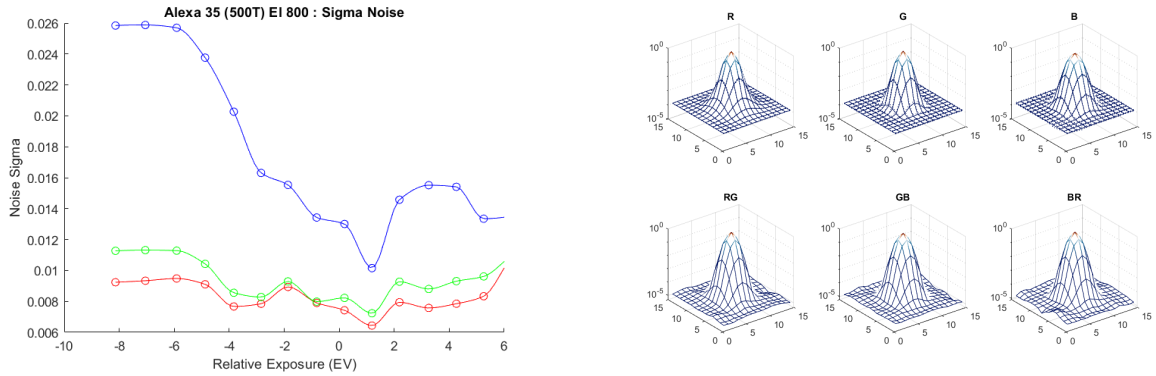

Figure 51 - Sigma Noise and Spatial Correlation of emulated film texture on Alexa 35 @ EI 800

As a reminder, 5OOT was measured as

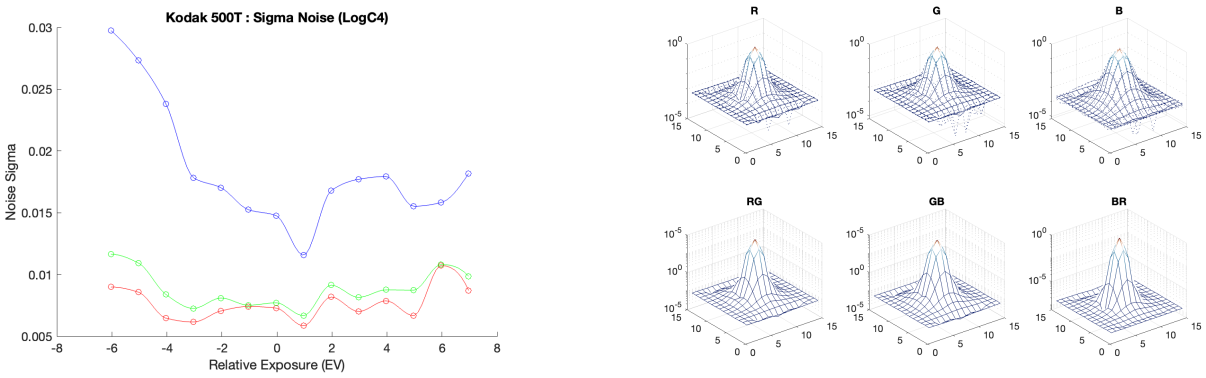

Figure 52 - Sigma Noise and Spatial Correlation of 500T

We can notice that the emulation is a success both in terms of power and spatial correlation. Discrepancies in the visualization of spatial correlation are due to negative values in the film AutoCorrelation and the log plot. Higher EI values are more challenging as the sensor noise starts to disrupt the synthesized grain. Indeed, while not being displayed in this thesis, EI 3200 noise is not fully covered by 500T emulation, especially in the low-mid range.

RoD lowers grain as it is based on Gaussian filtering kernels, but the effect is not sufficient.

6.1.2 MTF measures

Displayed here are artificial Edges (convolved with a kernel mimicking A35 OLPF) processed with RoD algorithm side by side with original Film MTF for various exposures (-3,0,+3)

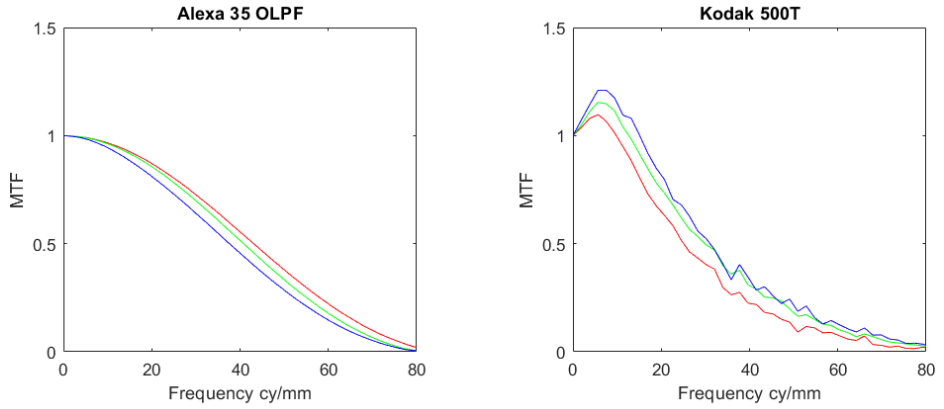

Reference Input
MTF - Exp0

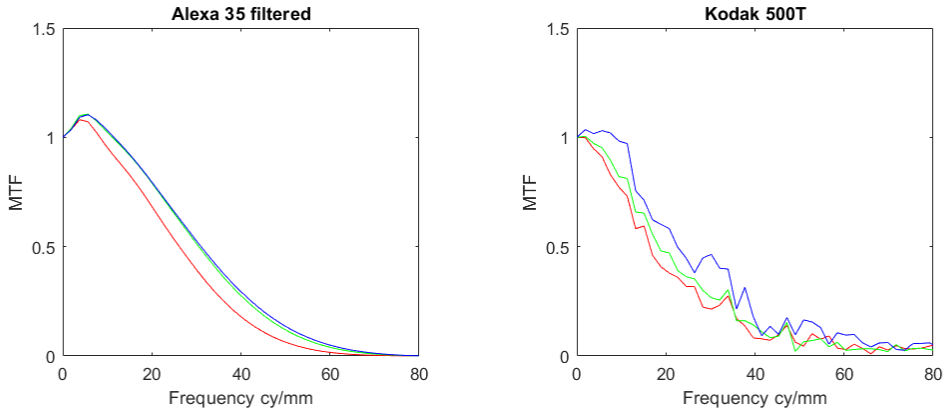

Filtered Edge
MTF - Exp-3

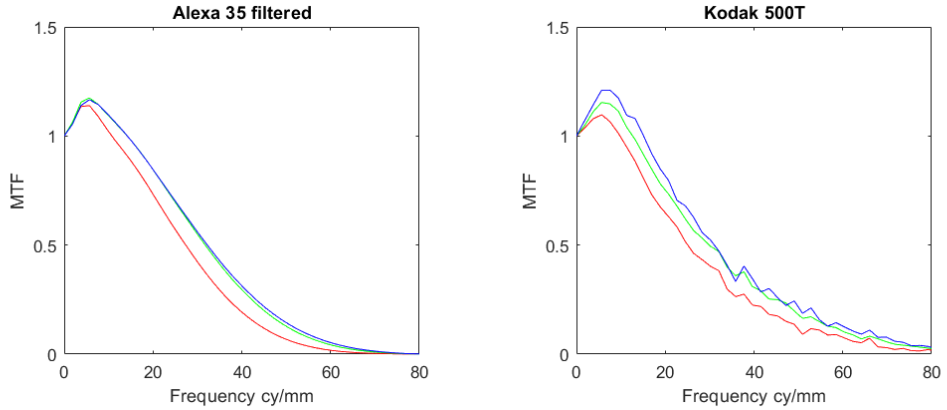

Filtered Edge
MTF - Exp0

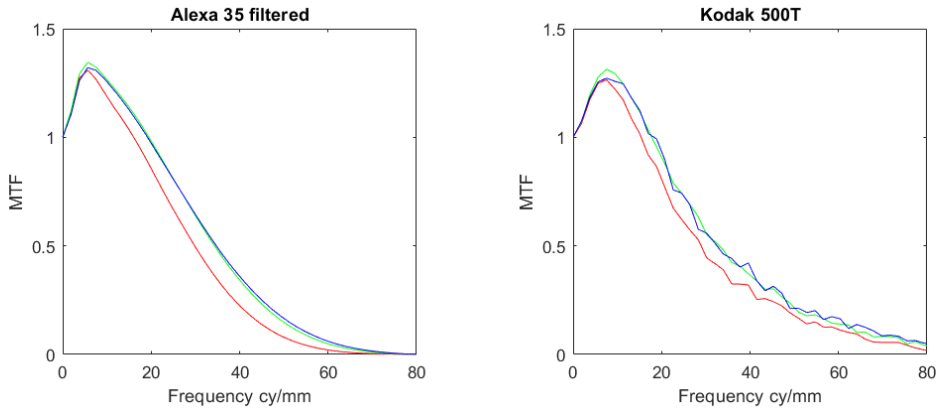

Filtered Edge
MTF - Exp+3

Figure 53 - MTF measurement of Edge filtered by the RoD algorithm

6.1.3 Color evaluation

These ΔE2000 has been computed between Kodak 500T and Alexa35 corrected with different degree of RPCC.

	NoCorrection	3x3 Matrix	RPCC degree 2	RPCC degree 3
Mean ΔE2000	3.69	2.22	2.04	1.93
Best 90%	3.31	1.89	1.74	1.65
Worst 10%	7.15	5.14	4.79	4.47

Figure 54 - ΔE2000 from different RPCC Degree

6.2 Visual evaluation

Figure 55 -Pairs of Edges : Processed Alexa35 Edges (bottom) And Film Edges (top) - Exposures -3,0,+3,+5 EV Grain free

This section presents the visual results of the emulation synthesis that we created through this thesis. Edges (Fig. 55) are synthetic and pre-filtered to match the Alexa OLPF. The film edges are the results of a concatenation of the ESF.
Results on real images are not color corrected but benefit from the full emulation pipeline with RoD filtering Halation and to Noise addition. Additional processed footage may be given to the reader if asked.

Figure 56 - Crops of assessment footage - Film (top) Processed Alexa 35 (bottom).

7 - Practical Work : Omniprésence de la Mine

La littérature conventionnelle de traitement des images fait référence à la texture comme caractéristique du sujet photographié. Cependant, dans ce mémoire, nous avons abordé la texture photographique se définissant en partie comme étant intrinsèquement lié au support de captation. Il nous a en effet paru important d'apposer à la définition stricto sensu, des notions décrivant le caractère visuel singulier apporté ni par l'objectif ni par le sujet, mais dépendant uniquement du support de captation et de ses spécificités. En photographie analogique, on rencontre alors des caractéristiques visuelles apportées par la matérialité du support, notamment son épaisseur, mais plus essentiellement la diversité en taille de ses cristaux sensibles. Cette répartition stochastique responsable de la captation des photons, mais également du bruit analogique présent sur l'image finale tranche radicalement à la matrice de captation ordonnée et sans épaisseur en photographie numérique. La texture de l'image numérique ne dépend alors plus de son support et de sa matérialité. Néanmoins, en dépit d'une image immatérielle tant visuellement que techniquement, la caméra et le processus de traitement numérique dépend eux de ressources matérielles tangibles et mesurables. La mine, absente de nos imaginaires collectifs, s'immisce pourtant dans la totalité des activités humaines. Paradoxalement, la dépendance à la Terre et ces ressources minières est importante et grandie à mesure que nous dé-matérialisons nos données, nos services et nos pratiques. Délocalisées au profit du marché libre, la Mine et ses grandes industries ne sont plus en Europe et leur absence accentue ce paradigme dé-matérialiste. Des traces et vestiges de la mine ont cependant subsisté et marquent avec véhémence les territoires qu'elle a un jour écorchés. De plus, la mine n'est pas complètement sortie d'Europe et compte d'ailleurs y revenir pour en renforcer la souveraineté.

Ce projet documentaire se présente comme une représentation de la mine en Europe de l'Ouest. En faisant un détour par la Pologne est l'Allemagne, Omniprésence de la Mine se concentre sur les territoires du Massif Central et des Pyrénées. La géologie y

étant diversifiée et les terres pas toujours évidentes à cultiver, se sont développées des mines de tout métaux et minerais. Certaine exploitation remonte jusqu'à l'antiquité, mais la plupart ont été pleinement exploitées depuis la révolution industrielle. Le charbon, qui en est la représentation ultime, a commencé à être exploité dans les Houillères de la Loire avant de s'étendre à l'Auvergne, au Midi-Pyrénées et aux Cévennes. Sur des modèles et apparences similaires existent également des exploitations de minerai métalliques. Du Zinc au Plomb en passant pas l'Or et l'Arsenic, les métaux sont souvent exploités ensemble et nécessitent un raffinage couteux pour en extraire les infimes quantités contenues dans la roche. Les déchets sont difficiles à traiter et sont continuellement stockés dans des retenues, tas de stérile et autres déversoirs. Les conditions de travail, bien qu'hypothétiques, sont surement difficiles et les risques importants.

Conclusion and outlooks

Historically referring to scene characteristics, the notion of texture was not used to describe the spatial attributes of a light-sensitive material. If most photographers and cinematographers were sensitive to Grain and Rendition of Detail, they were not considering these film attributes as fully integrated into the notion of texture. Indeed, when digital cameras started to take over the cinema industry, a «Lack of Look» was described by numerous cinematographers, both color and texture wise. To remedy these spatial issues, vintage lenses started to be used with digital cameras to break their inherent sharpness. More recently, numerous plug-ins and software provided film emulation to recover the material depth that was lost with digital sensors. Post-houses also started to offer solutions and workflows integrating an analog intermediate to modify the spatial characteristics of the output material. In an era where uses are more and more becoming digital and intangible, a sense of materiality become increasingly valuable.

Being conducted at ARRI, this thesis was in direct contact with the needs of cinematographers. The thesis topic was even proposed by ARRI's Image Science Department as an exploration of the possibility and feasibility of film texture emulation.

Studying image processing for a semester at Sorbonne Université, I started exploring and determining what were the parameters influencing texture. After a few months of testing at ARRI, we agreed upon three main characteristics that were Grain, Rendition of Details and Halation. A set of tests and measurements were organized and fulfilled to acquire a dataset in order to extract those parameters. The analysis and synthesis were interdisciplinary, mixing both color and spatial processing, as well as requiring a good understanding and knowledge of film and analog sensitometry.

Given the outcomes of this thesis, we can confidently conclude that the task of recovering film texture has been successful in all regards. Yet, as with all research

works, improvement to achieve more faithful results can always be implemented and new or existing topics can be further explored.
Indeed, better protocols could be built both for color evaluation and MTF measurements. The first could largely benefit from actual spectral sensitivity measurement, as the latter could benefit from better management or correction of both optical aberrations and flare on the measured characteristics.
Furthermore, validation data with more film captured scenes and more rigorous assessment protocols could be largely improved, as explained in section 6. Last but not least, building a user-configurable data-driven synthesis model is the most important point that should be further developed in upcoming work. This would require extensive testing with a panel of observers to determine how to generalize and extrapolate discrete data acquisitions, as well as determining the acceptable range of operation for each parameter.

Nevertheless, the thesis provides a deep understanding of how film texture can be considered and modeled. It demonstrates the crucial role of materiality, in the sense of photosensitive crystals, dye clouds, film thickness and chemical effects in the restitution of scenes captured by color negative films. This perspective which constitutes the essence of this written work is carried out in the practical part of this thesis presenting images of the earth's crust and its resources. The "Omniprésence de la Mine" project explores the impact of mines of yesterday and tomorrow. It highlights that mining, the driving force behind all industrial processes, not only defines film texture, but digital photography too, as intangible as it seems.

List of Acronyms

ADA	ARRI Debayering Algorithm
AWG4	ARRI Wide Gamut 4
AWGN	Additive White Gaussian Noise
CFA	Color Filter Array
CDD	Channel Dependent Densities
CID	Channel Independent Densities
ESF	Edge Spread Function
FFT	Fast Fourier Transform
LUT	LookUp Table
LSF	Line Spread Function
MTF	Modulation Transfer Function
OLPF	Optical Low Pass Filter
PFE	Print Film Emulation
PSD	Power Spectral Density
PSF	Point Spread Function
RoD	Rendition of Detail
SNR	Signal to Noise Ratio

Glossary

Debayering

Debayering is the step that allows to recover missing values of an image coming from a Bayer pattern filtered sensor. The right term to use should be demosaicing as a bayer pattern is simply a type of color filtering array. Yet, because Bayer patterns are the most used CFA in the industry, the word debayering is largely accepted. Simple debayering can be linear and thus be easily reversed if the algorithm depends on a simple average method based on the neighborhood pixels. Yet, state-of-the-art debayering algorithms tend to be image content dependent such as edge maps, resulting in images less affected by moiré or spacial artifacts.

Fourier Transform

A Fourier transform is a mathematical operation that describes a signal with the frequencies it contains. In images, high frequencies represent sharp edges and small details (so mainly high contrast regions) and low frequencies represent low detail and homogenous regions.

LUT

A Lookup Table is an object that allows to store data and which main purpose is to match the input values to the output ones. These tables can have many dimensions and can be used for color management and more broadly other image processing tasks such as noise distribution.

Matrix

In Image processing, a matrix is an array composed of coefficients mixing the level of each color primary. Matrices are among the most basic color corrections in image processing. Standard Matrices are 3x3 and offer a linear combination of RGB primaries, but more evolved models can mix RGB and non-linear combinations of these primaries, such as root polynomial color correction matrices.

Tonal Curve - Tone Mapping

A tonal curve is a curve that describes the tonal gradation of an image. This curve is called linear when the digital gradation of the image is the same as the amount of light it received from the scene. In photography, raw files usually have a linear encoding, whereas cinema tends to encode with a logarithmic curve to counteract the over-quantization in highlights and gain weight on saved files.

Noise

Noise is defined as an unwanted, additional signal captured by a measuring device. There are different sources of noise such as photon noise, reading noise, thermal noise … More than different sources, noise can have multiple shapes, described thanks to its spectra. In most cases, noise usually reduces the readability of an image. Yet certain types of noise may be wanted to homogenize an image, enhance acutance or alternate their image on purpose. Furthermore, noise can allow to lower quantization banding and increase signal readability thanks to the stochastic resonance effect. It's physically impossible to achieve noise-free images without any image processing (denoising) thus making the discipline really attractive when such results want to be achieved.

Characteristic Curve - H&D Curve

The Characteristic Curve of a film is given by the amount of density produced by a developed film when exposed to a defined amount of light. The sensitometric response of a film is measured with a step wedge with a range of patches having a fixed delta of density separating them. The sensitometric response is used to define the sensitivity of a film according to ISO standards and allows to determine any defined metric for contrast measurement (gamma, Contrast Index …). Even if the name H&D seems to relate to H (luminance) and D (Density), it is actually attributed to Hurter & Driffield, founders of sensitometry.

List of Figures

Bibliography

Grain

- S. Eckel, P. Huthwaite, U. Zscherpel, A. Schumm and N. Paul, *Realistic Film Noise Generation Based on Experimental Noise Spectra*, in *IEEE Transactions on Image Processing*, vol. 29, pp. 2987-2998, 2020

- Hanson, Kenneth. (2001). *A Simplified Method of Estimating Noise Power Spectra.* Proceedings of SPIE - The International Society for Optical Engineering.

- A Newson, Julie Delon, B Galerne. *A Stochastic Film Grain Model for Resolution-Independent Rendering.* Computer Graphics Forum, 2017

- B. T. Oh, S. -m. Lei and C. . -C. J. Kuo, *Advanced Film Grain Noise Extraction and Synthesis for High-Definition Video Coding*, in *IEEE Transactions on Circuits and Systems for Video Technology*, vol. 19, no. 12, pp. 1717-1729, Dec. 2009

- J. C. K. Yan, P. Campisi and D. Hatzinakos, *Film grain noise removal and generation for color images*, Proceedings of the 1998 IEEE International Conference on Acoustics, Speech and Signal Processing, ICASSP '98 (Cat. No.98CH36181), Seattle, WA, USA, 1998, pp. 2957-2960 vol.5

Optic, Rendition of Detail & Halation

- W. F. Berg, *The Photographic Emulsion Layer as a Three-Dimensional Recording Medium*, December 1969 / Vol. 8, No. 12 / APPLIED OPTICS 240

- Roland, Jackson K. M., *A Study of Slanted-Edge MTF Stability and Repeatability.* édité par Mohamed-Chaker Larabi et Sophie Triantaphillidou, 93960L. San Francisco, California, USA, 2015.

- Estribeau, Magali, et Pierre Magnan. *Fast MTF Measurement of CMOS Imagers Using ISO 12333 Slanted-Edge Methodology.* Edité par Jean-Pierre Chatard et Peter N. J. Dennis, 243. St. Etienne, France, 2004

- Janecek, Martin, et William W. Moses. *Optical Reflectance Measurements for Commonly Used Reflectors. IEEE Transactions on Nuclear Science* 55, nº 4 (août 2008)

Colour

- R. C. Aster, B. Borchers, and C. H. Thurber, *Parameter Estimation and Inverse Problems, 2nd ed. Elsevier Inc.*, 2013

- Edward J. Giorgianni et Thomas E. Madden, *Digital color management : encoding solutions,* 2008, 415 pages, ISBN : 9780470512449

- Finlayson, Graham & Mackiewicz, Michal & Hurlbert, Anya. (2015). *Color Correction Using Root-Polynomial Regression.* IEEE transactions on image processing : a publication of the IEEE Signal Processing Society. 24. 1460-1470. 10.1109/TIP.2015.2405336.

- R.W.G Hunt, *The Reproduction of Colour, 6th Edition*, WILEY, 2004, 724 Pages, ISBN: 978-0-470-02425-6

Image Science

- J.C Dainty and R. Shaw, *Image Science : Principles, Analysis and evaluation of Photographic-Type Imaging Processes,* Academic Press, 1974, 402 pages

- Bergthaller, *P. Couplers in Colour Photography—Chemistry and Function Part 3. The Imaging Science Journal* 50, nº 4 (janvier 2002): 233-76.

- C. Noel Proudfoot. *SPSE Handbook of Photographic Science and Engineering second edition*. New York, IS&T, 1997, ISBN : 0-89208-198-8

- Thomas, Woodlief. *SPSE Handbook of Photographic Science and Engineering*. New York, Wiley, 1973.

- Andrews, Harry C, *Digital image restoration*, Englewood Cliffs, N.J. : Prentice-Hall, 1977

Technical Documentation & Norm

- Eastman Kodak Company, *The essential reference guide for filmmakers*, 213 Pages, 2007, Code: H-845

- KODAK Publication No. H-387*, KODAK Digital LAD Test Image, User's Guide and Digital Recorder Calibration and Aims, December 2011,* 5 pages

- KODAK, *KODAK VISION3 500T Color Negative Film 5219 / 7219 Datasheet,* Revised March 22, KODAK Publication No. H-1-5219, 4 pages

- KODAK, *Print Grain Index KODAK Publication No. E-58, July 2000*

- SMPTE, SMPTE ST 2065-2:2020, *Academy Printing Density (APD) - Spectral Responsivities, Reference Measurement Device and Spectral Calculation,* May 2020

- SMPTE, SMPTE ST 2065-3:2020, *Academy Density Exchange Encoding (ADX) Encoding Academy Printing Density (APD) Values,* September 2020

- Harald Brendel, Sean Cooper, *ARRI LogC4 Logarithmic Color Space Specification,* May 2023

- ARRI, ALEXA 35 *Software Update Package 1.2 User Manual*, July 2023

A - Appendix

Appendix 1

Edge attempt with a razor blade directly against a film. Diffraction effect is too strong

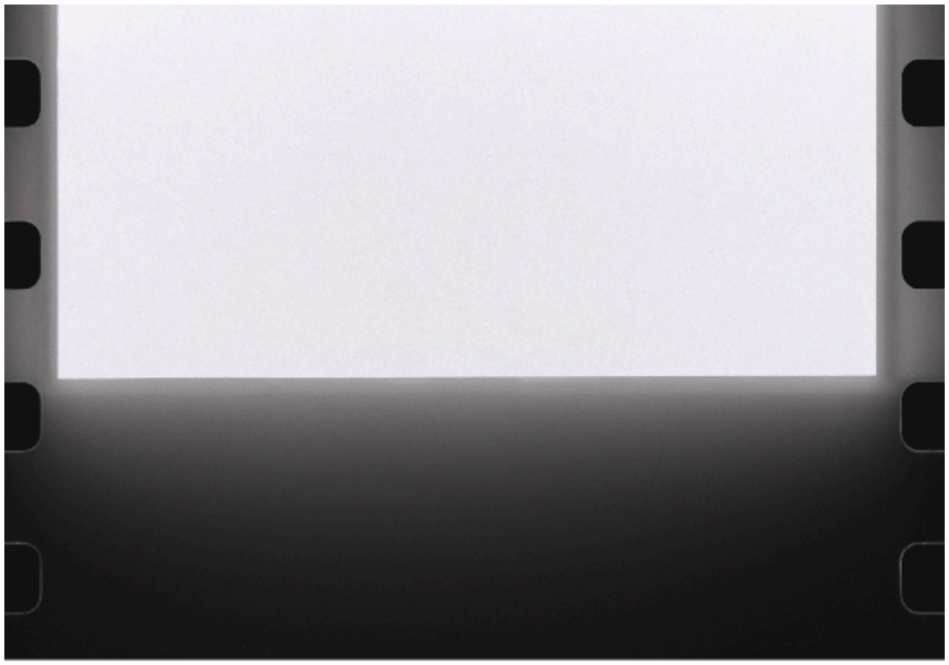

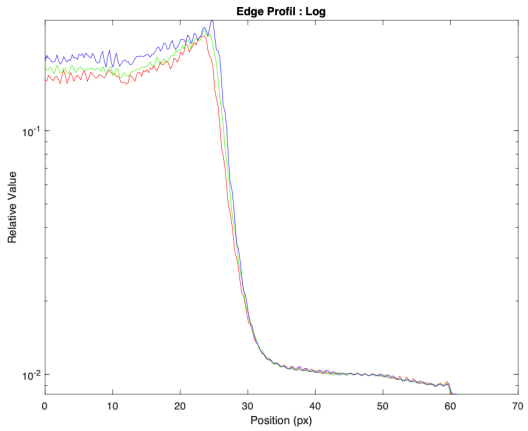

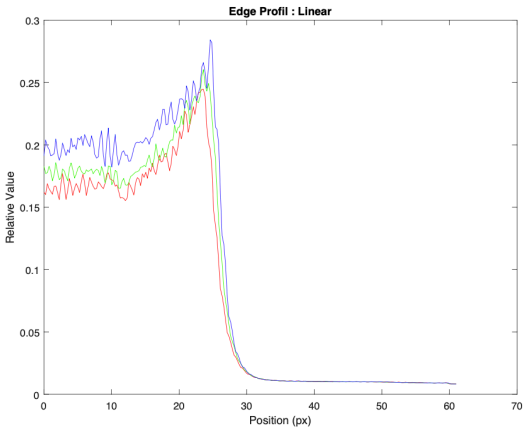

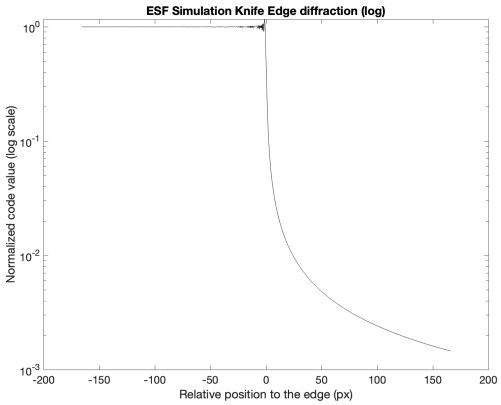

Appendix 2

MTF measurements according to a bracket position. Best Focus distance assessment.

Film

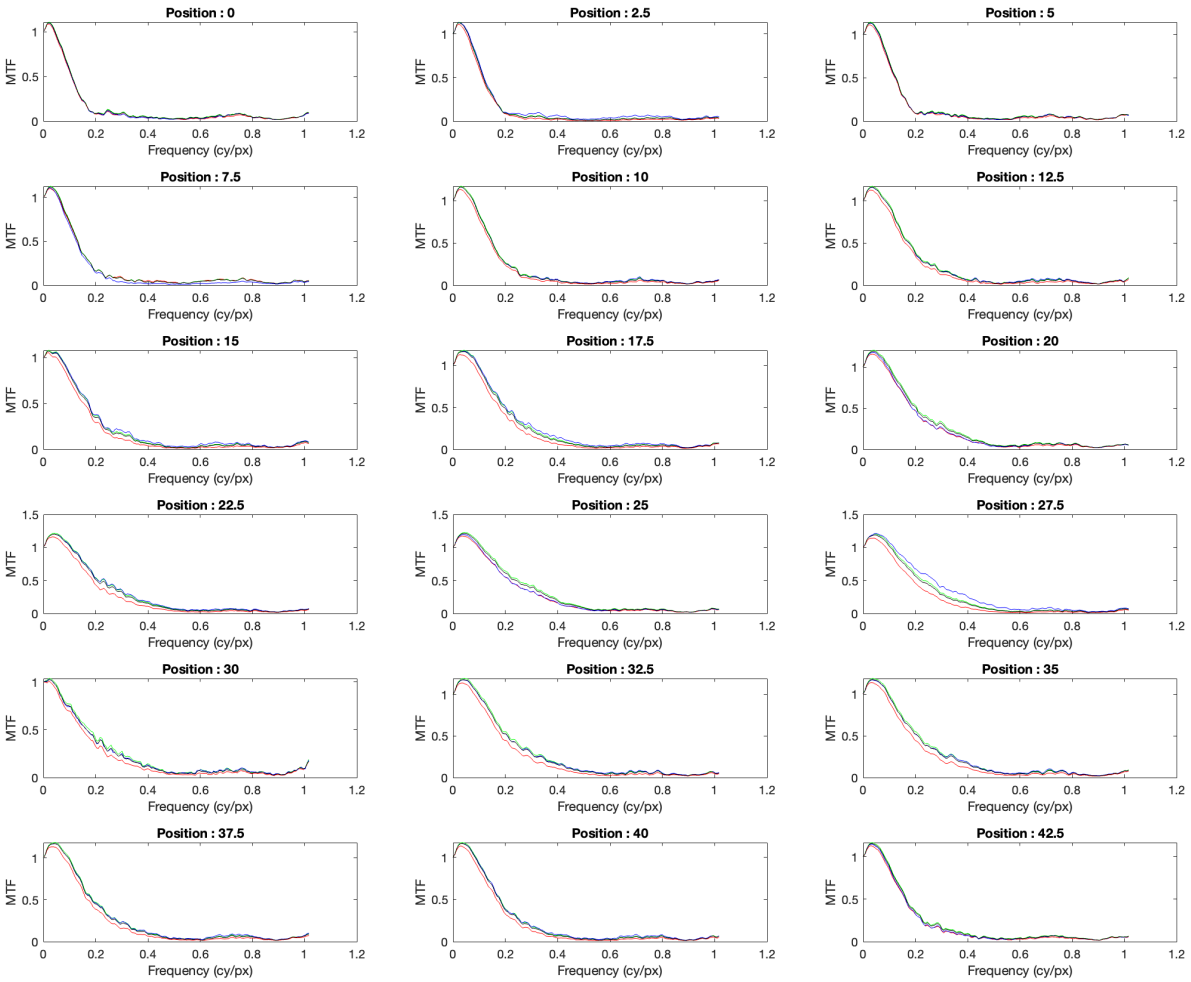

Digital

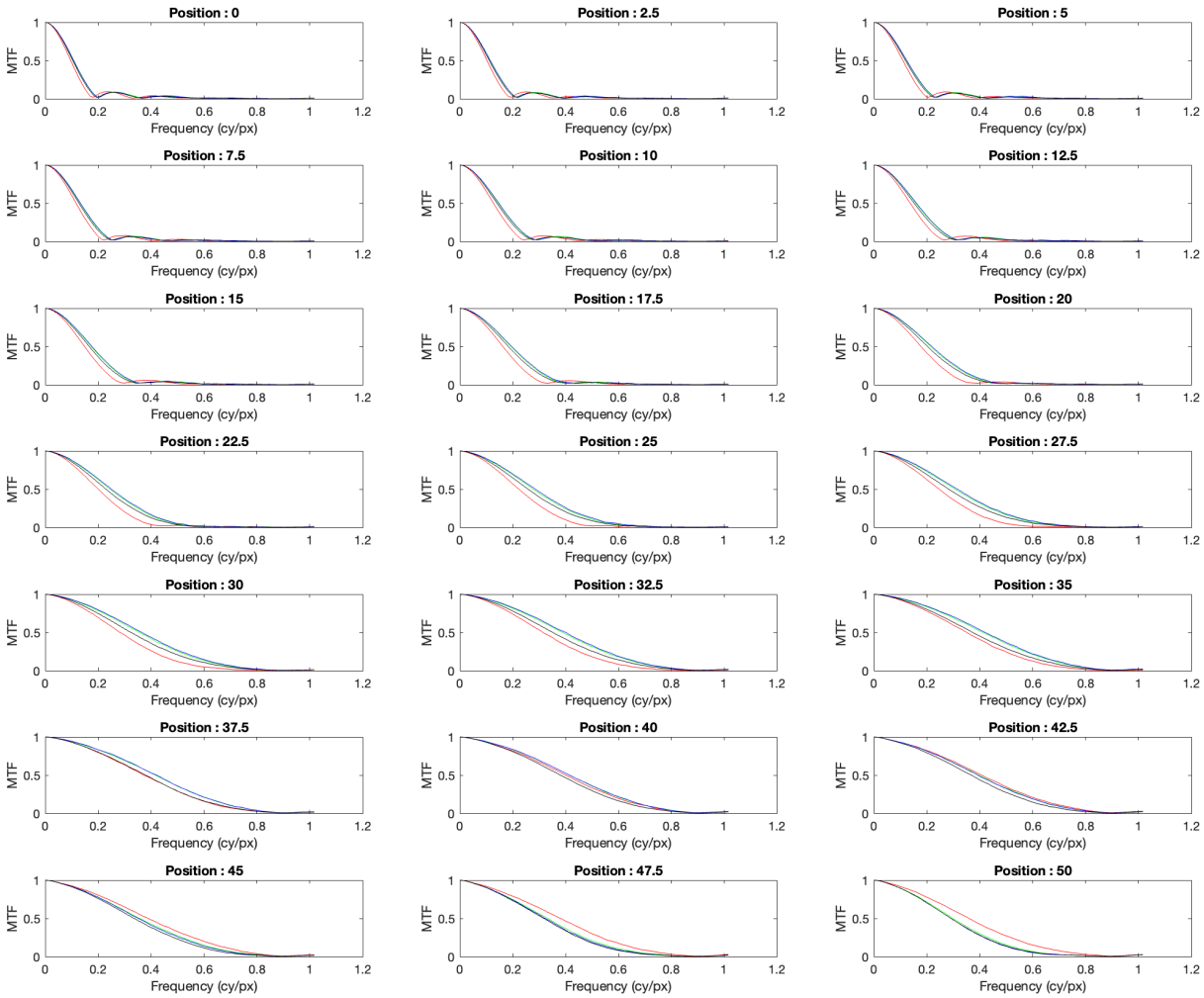
Position : 0
Position : 2.5
Position : 5
Position : 7.5
Position : 10
Position : 12.5
Position : 15
Position : 17.5
Position : 20
Position : 22.5
Position : 25
Position : 27.5
Position : 30
Position : 32.5
Position : 35
Position : 37.5
Position : 40
Position : 42.5
Position : 45
Position : 47.5
Position : 50
MTF
Frequency (cy/px)
0
0.5
1
0.2
0.4
0.6
0.8
1.2

Appendix 3

Original attempts of modeling the remjet with a Lambertian Kernel.

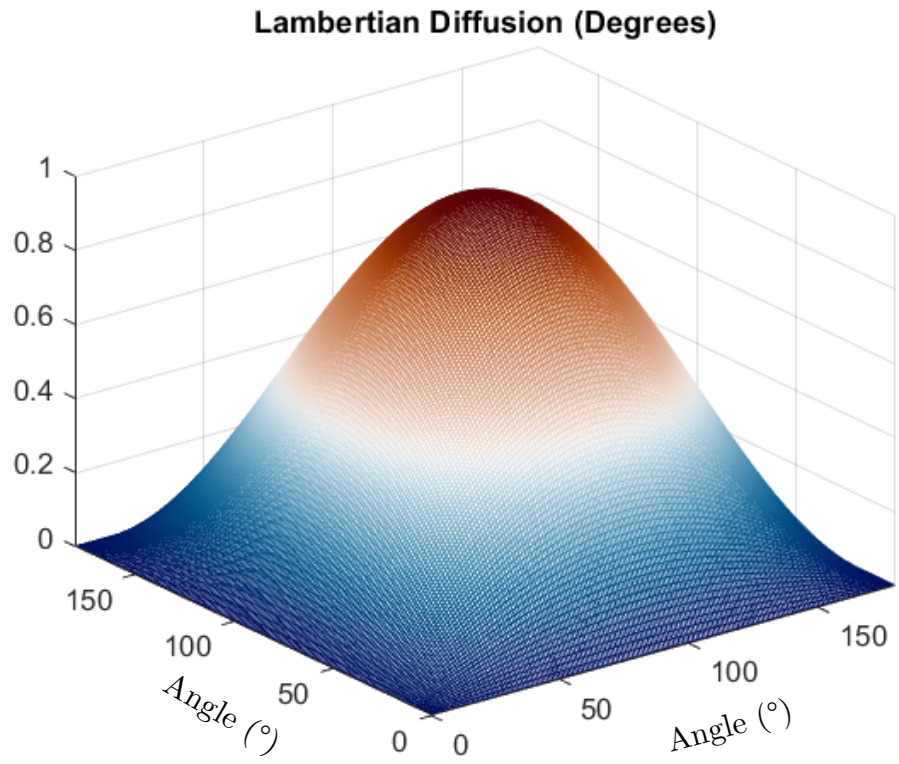

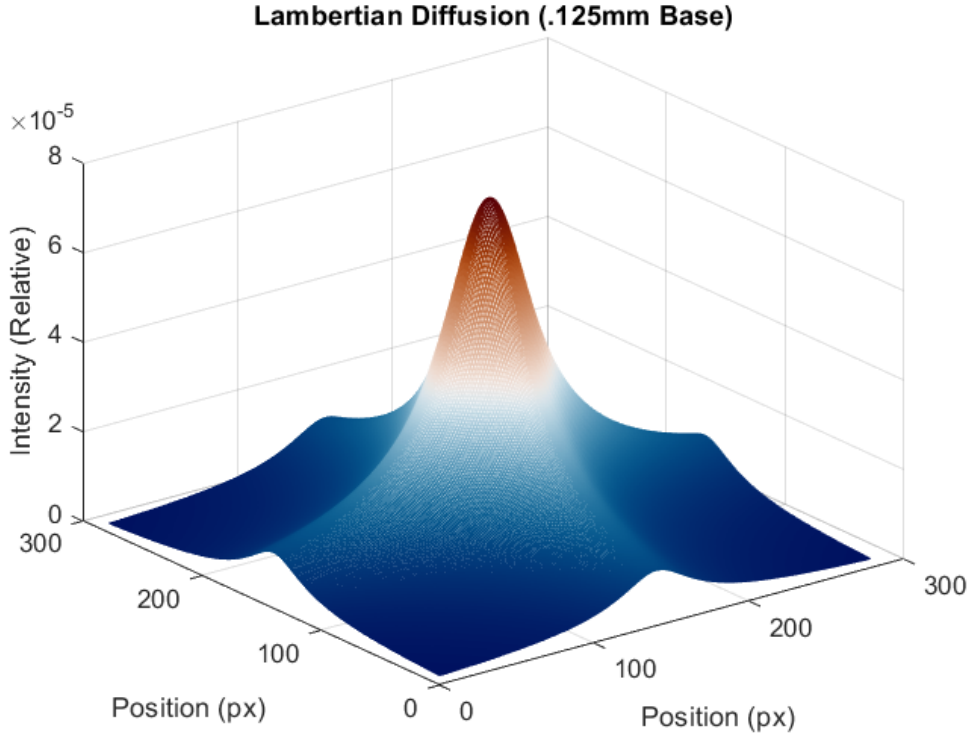

Appendix 4

Kodak 500T undeveloped, layers under a microscope. 2010 RL ShaneBrook

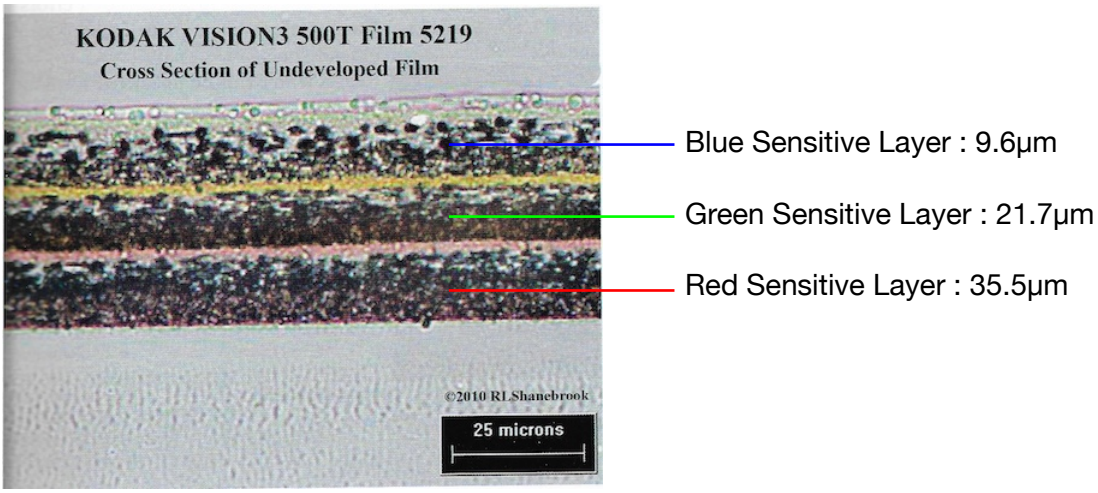

Appendix 5

Driving noise variance determination based on the variance of the sum of uncorrelated noises.

$$Var(R_d) = \frac{a^2(VarG_{input} - c^2VarB_{input}) + b^2(VarB_{input} - c^2VarG_{input}) + (c^4 - 1)VarR_{input}}{a^4 - 2(abc)^2 + b^4 + c^4 - 1}$$

$$Var(G_d) = \frac{a^2(VarR_{input} - b^2VarB_{input}) + b^4VarG_{input} - (bc)^2VarR_{input} + c^2VarB_{input} - VarG_{input}}{a^4 - 2(abc)^2 + b^4 + c^4 - 1}$$

$$Var(B_d) = \frac{a^4VarB_{input} + b^2(VarR_{input} - a^2VarG_{input}) - (ac)^2VarR_{input} + c^2VarG_{input} - VarB_{input}}{a^4 - 2(abc)^2 + b^4 + c^4 - 1}$$

Appendix 6

Overview of the processing pipeline, from input LogC4 to Output processed LogC4.